Optical Engineering

OpticalEngineering.SPIEDigitalLibrary.org

Recent advances in plasmonic nanostructures for sensing: a review

Pietro Strobbia
Eric Languirand
Brian M. Cullum

SPIE.

Optical Engineering 54(10), 100902 (October 2015)

REVIEW

Recent advances in plasmonic nanostructures for sensing: a review

Pietro Strobbia,[†] Eric Languirand,[†] and Brian M. Cullum[*]
University of Maryland Baltimore County, Department of Chemistry and Biochemistry, 1000 Hilltop Circle, Baltimore, Maryland 21250, United States

Abstract. This review describes the recent advances in plasmonic nanostructures for various sensing applications. In particular, significant advances in surface-enhanced Raman, surface plasmon resonance, and metal-enhanced fluorescence-sensing methodologies associated with the introduction of plasmonic nanostructures, made over the past decade, are highlighted. Plasmonic properties of the various nanostructures employed for each sensing technique are also tabulated to provide a systematic overview of the state-of-the-art in each sensing field. This review is not intended to be a comprehensive compilation of the literature but rather a critical review of the recent significant advances in plasmonic nanostructures for each sensing regime. [DOI: 10.1117/1.OE.54.10.100902]

Keywords: plasmonics; surface-enhanced Raman scattering; surface-enhanced Raman spectroscopy; surface plasmon resonance; metal-enhanced fluorescence.

Paper 150959V received Jul. 19, 2015; accepted for publication Sep. 2, 2015; published online Oct. 20, 2015.

1 Plasmonics

Nanotechnology has seen an exponential growth over the past two decades, largely due to the development of new materials as well as more advanced fabrication and characterization techniques.[1–3] Nanometric structures have been studied significantly over this time period due to the many unique phenomena that occur at this size scale (e.g., superparamagnetism, quantum confinement, plasmonics).[4–6] In particular, the unique interaction of light with metallic and semiconductor nanoparticles is a phenomenon that has been known for centuries; however, only recently has the name plasmonics been coined to categorize this rapidly growing field.[7–9]

The field of plasmonics represents the study of the interaction between light and conduction electrons of a metal.[6] These interactions in certain conditions lead to a collective excitation of conductive band electrons,[6] a surface plasmon (SP). This phenomenon involves photons and electrons coupling to form a hybrid between a light wave and an exited electronic level, producing an enhanced optical near-field at metallic interfaces (known as SPs) or within metallic nanostructures (known as localized surface plasmons; LSPs).[6,10] The energy of the SP resonance depends on the competing forces involved in the phenomenon, the excitation, and the nucleus–electron interaction. Variation of the shape, material composition, and number of structures can each greatly affect the resonance energy of this phenomenon.[11–14]

While coinage metals (i.e., silver, gold, copper) represent the most commonly employed plasmonic materials, due to the relationship between conductivity (i.e., electron losses) and SP magnitude, many other common and exotic materials have also been investigated over the past several decades.[13,15,16] The frequency of the SP depends on the conductive electron density of the material[6] causing analogous structures to exhibit SP at different wavelengths for different materials.[13,16] Figure 1 shows the SP-tuning ranges of several of the more common plasmonic materials studied to date.[15,16] As can be seen, gold and silver, while often exhibiting intense plasmons, are limited to the visible and near-infrared (NIR) region of the electromagnetic spectrum, whereas poor metals, such as aluminum, can sustain SPs in an extended region of the spectrum, but often with significantly reduced magnitudes.[15,16] In the case of gold, one of the longer wavelength materials, interband transitions dissipate the SP at wavelengths lower than 550 nm,[15,16] limiting its usefulness primarily to the red and NIR regions of the electromagnetic spectrum.

In addition to material composition, the shape and size of the material also play a large role in determining the optimal energy for exciting an SP.[11,12,17,18] Demonstration of this has been shown by investigating different size nanospheres as well as nonspherical particles (e.g., nanorods). An example of this shape dependence is shown in Fig. 2(a), which shows the optimal excitation wavelength dependence for longitudinal localized surface plasmon resonance (LSPR) of gold nanorods as a function of their relative lengths (as quantified by their aspect ratios, since their widths remain constant).[12,17] As can be seen from this plot, the SP wavelength of the longitudinal mode increases with increasing length. The experimental data (diamonds) are in good agreement with the theoretical values (solid line) derived from the Mie theory modified for spheroids.[17,21] A similar trend can also be seen in Fig. 2(b), where the SP absorption maximum of silver islands is plotted as a function of their size.[20] The silver island case is more complicated with respect to a single rod, but it reinforces the importance of the nanostructure size. As shown in Figs. 1 and 2, both shape and material play key roles in the plasmonic characteristics of a nanostructure.

Understanding and controlling the plasmonic characteristics of various nanostructured materials has resulted in significant advances in many areas, from sensing to light harvesting. In this review, we discuss the recent advances in the design of unique nanostructures aimed at generating more efficient plasmonic sensing platforms. This review will

*Address all correspondence to: Brian M. Cullum, E-mail: cullum@umbc.edu

[†]These authors contributed equally to this work.

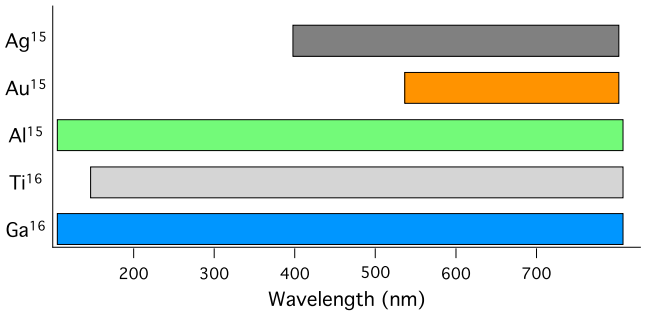

Fig. 1 Schematic diagram depicting the surface plasmon tuning ranges of common plasmonic metals.[15,16]

focus on significant recent advances in spectroscopic sensing techniques enabled by plasmonics. In particular, advances in plasmonic nanostructures for surface-enhanced Raman spectroscopy (SERS), surface plasmon resonance (SPR), and metal-enhanced fluorescence (MEF)-based sensing over the past decade will be covered.

2 Surface-Enhanced Raman Sensing

SERS was first observed in 1974, but its description as a unique plasmonic phenomenon was only made in 1977.[22–25]

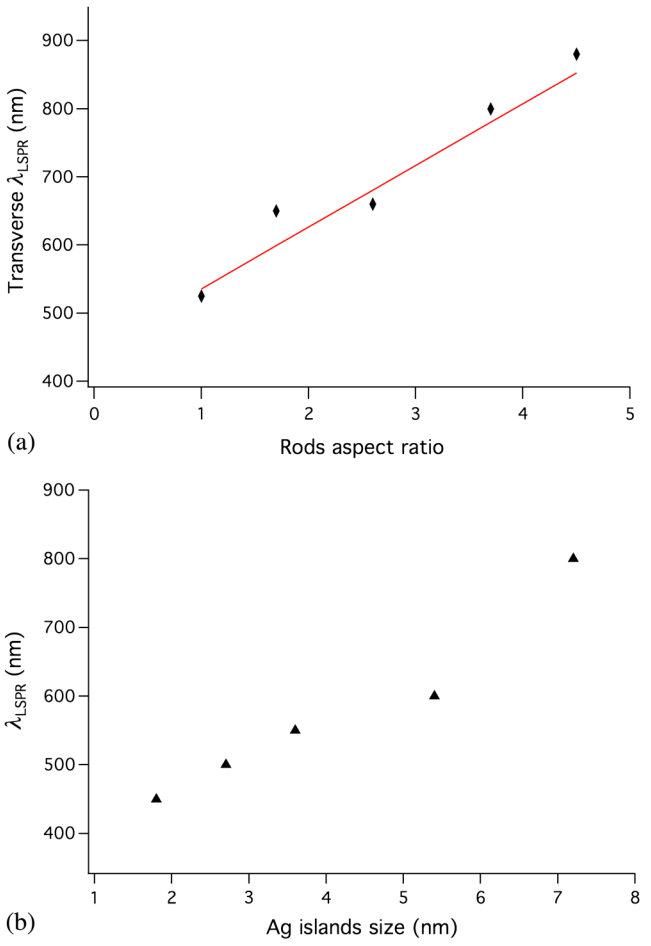

Fig. 2 (a) Experimental (diamonds) and theoretical predictions (solid line) of the maximum localized surface plasmon resonance (LSPR) wavelengths for gold nanorods of varying aspect ratio (calculated as longitudinal radius over transverse radius).[12,17,19] (b) Experimental wavelength of LSPR maxima for silver island films of different sizes.[20]

In the initial observations, molecules adsorbed on nanoscale roughened silver electrodes exhibited significantly enhanced Raman scattering compared to free molecules.[22] In the following years, the strong link between SERS and the nanostructure of the substrate, as well as its plasmonic characteristics, was theorized and described in detail.[26–29]

The enhancement mechanism of SERS has been historically divided into two processes,[30–32] a chemical (CHEM) enhancement and an electromagnetic (EM) enhancement. The CHEM enhancement is sample dependent and is commonly ascribed to the differences in the state of the molecule when in contact or in close proximity to a metallic surface.[33] These locations can generate variations in the Raman cross section as well as a shift for resonance Raman phenomena.[33] The CHEM enhancement process contributes to the total SERS enhancement by a factor of no more than 100–1000 typically.[34,35] The largest portion of the overall SERS enhancement is typically due to the EM enhancement that can amplify the Raman signal as much as $10^6 - 10^{11}$ fold.[34] The EM enhancement is strongly connected to the plasmonic characteristics, and the structure of the substrate used will be the principal focus of this part of the review.

The mechanism for the EM enhancement is based on the plasmonic nanostructure working as an antenna and amplifying the incoming and scattered radiation. Figure 3 shows a schematic representation depicting this enhancement process. The incoming radiation excites an SP on the nanoparticle/nanostructure, which generates an oscillating field of the same frequency but of increased intensity.[6,36] This effect exists in close proximity to the metallic surface and decays rapidly with distance.[37] Since the Raman scatter is proportional to the intensity of the field the analyte molecule experiences, there is a need in SERS for close contact between the analyte and the nanoparticle surface. In addition to the incident (i.e., excitation) light, the scattered light can also couple with the nanoparticle, further amplifying the resulting scattered radiation.[30] This second interaction suggests that the optimum SERS substrates would have an SP absorption that overlaps both the observed Raman band and the excitation wavelength.[31,38] For example, for SERS substrates intended to enhance the fingerprint region of a Raman spectrum and employing a 633-nm laser as the excitation source, an SP absorption band in the 644 to 679 nm range would be ideal.

In addition to simply determining the optimal SP excitation wavelength, the use of different metals and nanostructures for SERS substrates can also influence many other critical sensing parameters, including the metal surface accessibility for direct contact with an analyte, the surface area for analyte interaction, as well as the localized focusing of the electric field. All of these interrelated phenomena must be considered for the particular sensing application desired. For instance, gold is considered as a superior material for many applications due to its inertness, whereas silver, copper, or aluminum SERS nanostructures can present a challenge due to their rapid oxidation in ambient conditions. Alternatively, the EM enhancement obtainable for each metal is different due to interband transitions and other loss sources.[16,39] This can be seen in Fig. 4, which shows that comparable plasmon-optimized SERS substrates prepared with either gold, silver, or aluminum result in over two orders of magnitude greater SERS enhancement for the silver-based substrates (following visible excitation) than the next best

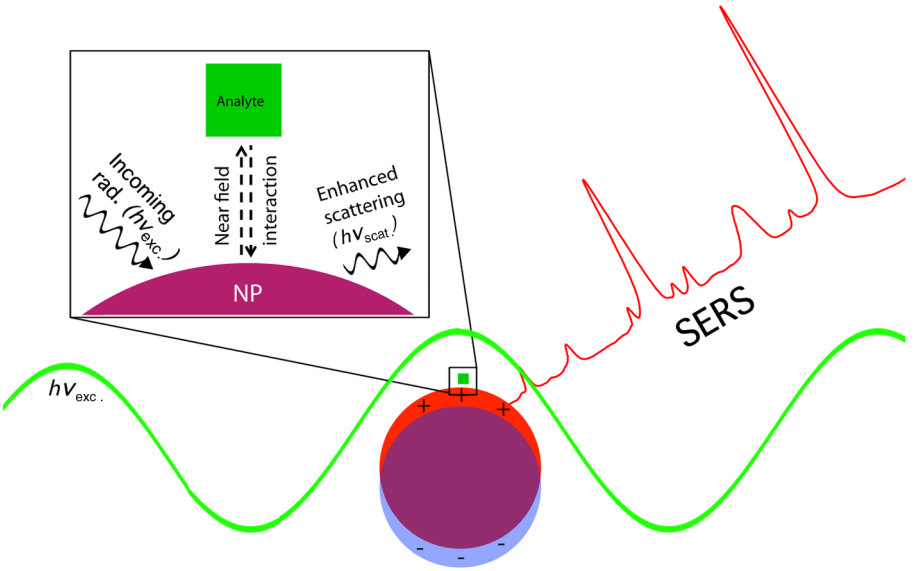

Fig. 3 Schematic diagram depicting the electromagnetic enhancement of surface-enhanced Raman spectroscopy (SERS). Incoming radiation of resonant wavelength ($h\nu_{exc.}$) interacts with the nanoparticle, exciting an LSPR. The near-field interaction between the Raman scatterer (i.e., analyte) and the plasmonic nanostructure increases the intensity of the scattered light ($h\nu_{scat.}$).

material (i.e., gold), and better still when compared to non-coinage metals.[12,39,40]

2.1 *Traditional SERS Nanostructures*

Although a large number of different types of nanostructured SERS substrates exist, with their numbers continuing to expand, they can typically be classified as belonging to (or evolving from) two different categories: (i) individual or randomly oriented aggregates of nanoparticles or (ii) ordered arrays of nanoparticles.

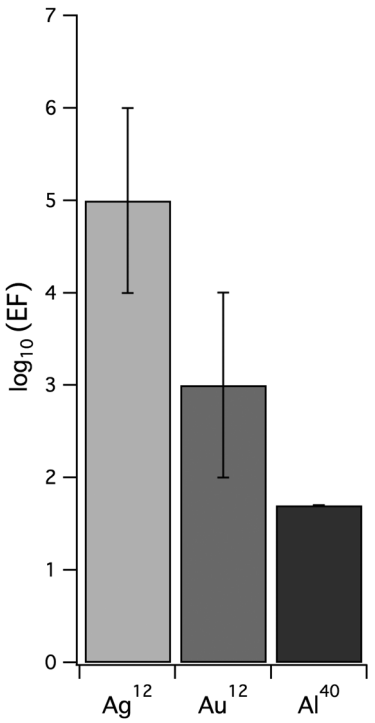

Fig. 4 Histogram showing the relative enhancement factors of comparable, plasmon-optimized SERS substrates made from silver, gold, and aluminum.[12,40]

2.1.1 *Individual/randomly orientated nanoparticles*

Individual nanoparticles and random aggregates of nanoparticles (e.g., colloids) have long been used to perform SERS sensing due to their small size and their large enhancement potential. Individual spherical metallic nanoparticles (e.g., individual colloidal particles) have been demonstrated (both theoretically and experimentally) to be capable of providing enhancement factors (EF) as great as 10^6.[34,39,41] This significant enhancement is due to the localization of the SP on the nanoparticle, resulting in a dramatically increased local electric field. This effect is further enhanced using nanoparticles with edges (e.g., nanorods) that are capable of focusing the charges (i.e., electric field) to specific locations on the nanoparticle via the "lightning rod" effect.[34,42–44]

In the 1990s, SERS enhancement factors as great as 10^{14-15} were measured using colloidal aggregates of metallic nanoparticles, allowing for Raman scatter from individual molecules to be measured.[45–47] These extreme SERS signal EF arise from the interaction of the overlapping electric fields of adjacent nanoparticles that were excited parallel to the interparticle axis, generating greatly enhancing regions between the nanoparticles known as "hot spots."[30,48] Unfortunately, the ability to reproducibly and controllably generate these localized "hot spots" has proven difficult, resulting in extremely irreproducible SERS enhancements from such aggregates.[49] For these reasons, many of the most recent advances in SERS sensing have revolved around nanoparticle fabrication methods focused on generating sharp intraparticle edges as well as methods of inducing organized aggregation of nanoparticles.

2.1.2 *Ordered nanostructure arrays*

To avoid the reproducibility issues associated with individual and random aggregates of SERS nanoparticles (e.g., colloidal

suspensions), ordered arrays of nanoparticles have also been explored over the past three decades, with the most common including electron beam lithography (EBL) arrays,[50] metal island films,[51–53] metallic films over nanospheres/nanostructures (MeFON),[51,54] and nanosphere lithography (NSL) arrays.[11,55] Although these systems typically exhibit lower SERS enhancement factors (typically 10^3 to 10^8)[52,56] than colloidal nanoparticle aggregates, they can exhibit uniform EF across extended areas (<10% RSD),[57] thereby providing a suitable surface for quantitative SERS analyses. In addition, each of these methods also provides a relatively simple means of controlling the optimal plasmon excitation wavelength for the array.[19,58] In the case of EBL, the precise control of the size of lithographically produced nanostructures provides plasmon tunability, while the amount of metal evaporated and the size of the underlying nanostructures employed in metal island films, MeFON, and NSL allow for precise control of the optimal plasmon excitation wavelength. Recent advances in plasmonic arrays for SERS sensing (described in Sec. 2.2) have focused on improving the SERS enhancement factors achievable using shapes and materials (i.e., mixed metals), while retaining the precise control possible with these extended surface substrates.

2.2 *Recent Advances in SERS Nanostructures for Sensing*

The most significant recent advances in plasmonic nanostructures for SERS sensing over the past decade have revolved around: (i) the use of mixed materials for increased signal enhancement, sample compatibility, and/or recyclability; (ii) the optimization of fabrication methods for the synthesis of irregular-shaped nanoparticles; and (iii) the fabrication of organized arrays of nanoparticles. Section 2.2.1–2.2.3 highlights the most significant recent advances in plasmonic nanostructures for SERS sensing. Table 1 provides a summary of the properties of these new plasmonic SERS nanostructures as well as a comparison to comparable figures of merit from traditional SERS structures. From this table, the trends of structure size versus plasmon absorption maximum and material versus plasmon absorption maximum can easily be seen for many different architectures. In addition, the original references to these structures are also provided for rapid access to fabrication details.

2.2.1 *Mixed materials*

Due to the strong influence the physical properties of the metal within which the plasmon is supported and the immediate surrounding play on the magnitude and shape of the resulting electric field, many recent advances have been made using mixed material nanostructures for enhanced SERS sensing. Structures fabricated with multiple materials have been exploited to tune the plasmonic characteristics of the substrates to increase local electric field strengths or add functionality. These mixed material substrates include (i) dielectric materials coated with metals,[62–64,70] (ii) metals coated with dielectrics,[53,71–74] (iii) semiconductors coated with metals,[75,76] and (iv) multilayered metal structures separated by dielectrics.[57,77–80]

One of the earliest and most prominent classes of these mixed material nanostructures for SERS sensing is known as core–shell nanoparticles, which consist of a dielectric core structure coated with a metallic shell [see Fig. 5(a)]. Often consisting of a silica nanoparticle core and coated by metal via chemical reduction of metal salts, these nanoshell structures provide the ability to tune their LSPR absorption maxima by modifying the core/shell radii ratio.[17,70,81,82] Unlike colloidal metal particles, these core–shell nanostructures allow for fabrication of nanoparticles for SERS applications that can be tuned for optimal excitation with various wavelengths without a concomitant change in particle size. Furthermore, the presence of the dielectric core helps localize the SP to the metal surface, resulting in larger electric fields and corresponding EF with respect to comparable metal nanoparticles.[62,64]

In addition to providing a controllable means of tuning the plasmon absorption wavelength and enhancing the electric field at the sensing surface, dielectric shells have also been used in SERS substrates to provide a protective layer for both the local environment being sensed as well as the metal surface itself.[53,71–74] Recently, shell isolated nanoparticle-enhanced Raman spectroscopy (SHINERS) was developed, in which ultrathin layers of metal oxides (e.g., Al_2O_3, SiO_2, MgO) are uniformly coated on underlying SERS nanoparticles via atomic layer deposition (ALD) and chemically to protect them from the often oxidizing environment of the sample.[73,74] With many of the best SERS-enhancing metals (i.e., silver and copper) often suffering from rapid degradation in SERS enhancement due to oxidation of the plasmon-supporting metal surface, such metal oxide-coated nanoparticles have resulted in significantly increased usage times. By employing ultrathin coating methods with high conformity (e.g., ALD), the decrease in electric field strength at the sensing surface can be minimized, resulting in SERS enhancement factors not much lower than comparable uncoated nanoparticles.[53] In addition to protecting the surface from oxidation, such ultrathin surface coatings have also been demonstrated to reduce aggregation of particles by reducing interparticle surface interactions, resulting in isolated particles that can be used in applications where aggregates are not suitable.

Aside from employing mixtures of dielectric materials with metals, plasmonic nanostructures consisting of semiconductor materials coated with thin metallic layers have also been developed and demonstrated for SERS sensing. By fabricating plasmonic nanostructures with a TiO_2 or ZnO core and a thin metal coating, "self-cleaning" SERS nanostructures can be generated.[75,76] In the case of these particular semiconductors, exposure to UV light results in the release of oxidizing electrons[76] that can travel through the thin conductive metallic shell, removing adsorbed materials and allow for regeneration of the SERS active surface. While such SERS nanoparticles address a common problem in SERS sensing (i.e., substrate reusability) and have demonstrated the capability of being reused multiple times, the thin metal surface is susceptible to flaking during the regeneration cycle and is not capable of removing tightly bound species, potentially limiting their applicability.

In addition to employing a single layer of dielectric material and a single layer of metal for SERS substrate fabrication, alternating layers of metal, dielectric, and metal have also been employed to provide significantly greater SERS enhancements (see Fig. 6).[57,77–80] Such multilayer geometries have been employed on silver island films[77] and MeFON surfaces,[57,78,79,83] demonstrating the versatility of this enhancement mechanism. In particular, by applying

Table 1 Properties of plasmonic nanostructures for SERS.

Nanostructure type	Metal	Size/dia. (nm)	λ_{LSPR} (nm)	EF	$\lambda_{exc.}$ (nm)	References
Particle	Ag	10 to 25	—	10^6	407	59
		33	420	10^{4-6}	633	12
		50	~405	1.1×10^5	633	60
		50	~405	2.2×10^5	785	60
	Au	60	540	10^3	514	47
		29	520	10^{2-4}	633	12
		15	520	5.1×10^2	532	43
		15	520	3.8×10^2	785	43
Colloidal aggregates	Ag	10 to 25	—	10^{14}	830	59
		10 to 25	—	10^{7-8}	407	59
		36	405	—	514	61
	Au	60	540	10^{14}	830	47
Rod	Ag	$h = 43$	535 (long.)	10^{3-6}	633	12
		$w = 12$	420 (trans.)			
		$h = 214$	615 (long.)	10^{5-7}	633	12
		$w = 20$	420 (trans.)			
		$h = 60$	600 (long.)	7.7×10^4	785	44
		$w = 21$	535 (trans.)			
		$h = 100$	775 (long.)	2.9×10^5	785	44
		$w = 6$	535 (trans.)			
	Au	$h = 41$	650 (long.)	10^{3-5}	633	12
		$w = 24$	520 (trans.)			
		$h = 57$	850 (long.)	10^{2-4}	633	12
		$w = 13$	520 (trans.)			
		$h = 372$	>1200 (long.)	10^{2-4}	633	12
		$w = 23$	520 (trans.)			
		$h = 70$	800 (long.)	—	—	19
		$w = 19$	525 (trans.)			
		$h = 30$	715 (long.)	1.6×10^3	785	43
		$w = 9$	520 (trans.)			
		$h = 30$	715 (long.)	5.1×10^4	532	43
		$w = 9$	520 (trans.)			
Klarite®	Au	—	~600	10^{4-6}	633	58

Table 1 (*Continued*).

Nanostructure type	Metal	Size/dia. (nm)	λ_{LSPR} (nm)	EF	$\lambda_{exc.}$ (nm)	References
Island films	Ag	3.5	~550	4.8×10^4	514	51
		3.5	~550	7.1×10^4	641	51
		3.5	~550	9.7×10^4	722	51
		8	~700	9.5×10^4	514	51
		8	~700	2.4×10^5	641	51
		8	~700	5.3×10^5	722	51
		100	—	4.3×10^5	1064	52
	Au	68	—	6.0×10^3	1064	52
MeFON	Ag	200 (metal)	—	1×10^7	753	51
		542 (sphere)				
Nanosphere lithography	Ag	18 (metal)	426	—	—	11
		542 (sphere)				
		14 (metal)	565	—	—	11
		165 (sphere)				
		18 (metal)	747	—	—	11
		264 (sphere)				
		55 (metal)	810	10^8	770	56
		450 (sphere)				
Shell	Ag	78 (core)	—	4.8×10^9	782	62
		92 (shell)				
		116 (core)	~850	5.0×10^9	782	62 and 63
		138 (shell)				
		162 (core)	—	2.5×10^{10}	782	62
		182 (shell)				
		188 (core)	~950	2.4×10^{10}	782	62 and 63
		214 (shell)				
	Au	80 (core)	660	—	—	19
		100 (shell)				
		98 (core)	~700	—	—	64
		140 (shell)				
		120 (core)	725	—	—	65
		160 (shell)				
		150 (core)	910	—	—	65
		170 (shell)				
		340 (core)	1500	—	—	65
		360 (shell)				
Multilayer	Ag	100	650	5×10^7	633	57

Table 1 (*Continued*).

Nanostructure type	Metal	Size/dia. (nm)	λ_{LSPR} (nm)	EF	$\lambda_{exc.}$ (nm)	References
Aligned rods	Ag	$h = 868$	1056 (long.)	5×10^8	785	66
		$w = 99$	357 (trans.)			
INRA	Ag	390 (sphere)	~475	1.3×10^7	633	67
		600 (sphere)	~800	4.9×10^7	785	67
		790 (sphere)	~1100	1.0×10^8	1064	67
Nanostar	Au	~50	~800	3×10^4	633	60
		~50	~800	4×10^5	785	60
		~34	675	3.9×10^3	532	43
		~34	675	1.0×10^5	785	43
OWL	Au	$h = 60$	785	10^9	785	68
Nanofingers	Au	$h = 700$	750	2×10^{10}	785	69
		$w = 100$				

this multilayer geometry to MeFON substrates, it is possible to further enhance the original SERS signal of these substrates by over two orders of magnitude.[79] These structures are fabricated by growing ultrathin metal-oxide spacers over an MeFON substrate and subsequently depositing another metallic film.[57,84] The overall enhancement generated is dependent on the number of alternating layers of metal and dielectric employed and not the overall size. This means that by applying additional thinner layers, the SERS enhancement can be increased independent of the underlying structure, making it a viable means for further enhancing many different types of SERS substrates.

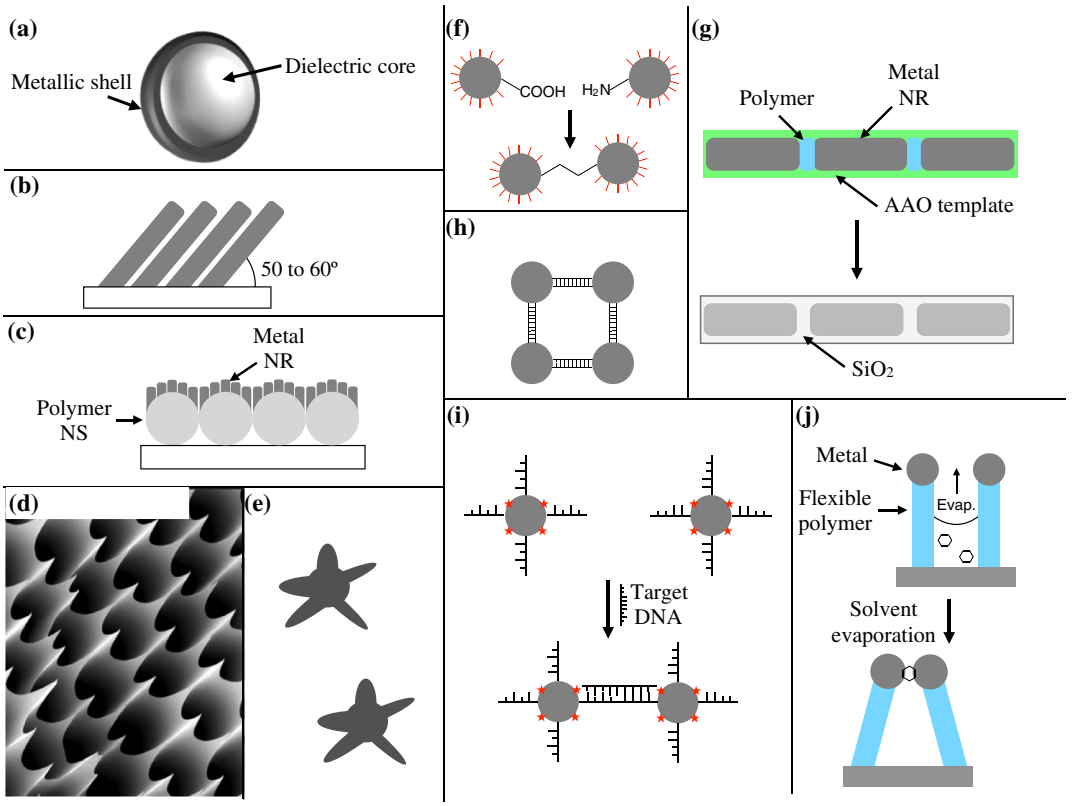

Fig. 5 Schematic images depicting recent plasmonic nanostructures developed for SERS sensing, including (a) core–shell nanoparticles, (b) aligned nanorods, (c) immobilized silver nanorod assemblies (INRA), (d) fiber bundles, (e) nanostars, (f) controlled dimers, (g) on-wire lithographic (OWL) structures, (h) DNA origami, (i) induced aggregation, and (j) nanofingers.

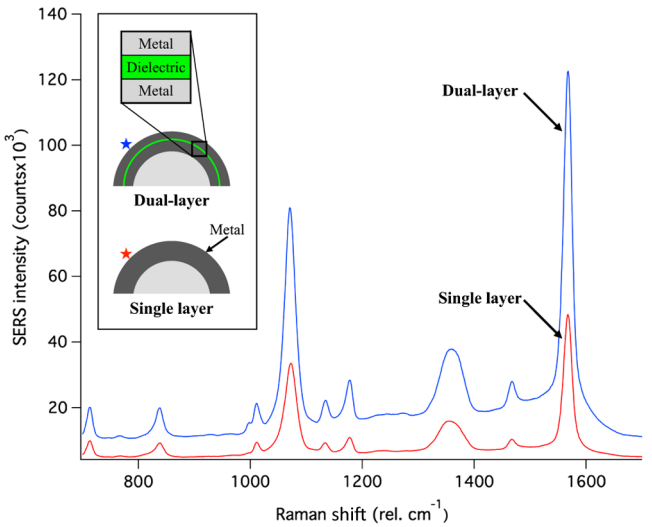

Fig. 6 SERS spectra of mercapto benzoic acid on MeFON substrates made with a single silver film (bottom spectrum) and a dual-layer film (top spectrum), demonstrating the multilayer enhancement effect. Inset is a schematic diagram of the associated single and dual layer plasmonic structures.

2.2.2 *Irregular shapes*

In addition to improve SERS enhancement factors by altering the material composition of the plasmonic nanostructures, fabrication methods for generating structural motifs resulting in sharp predictable edges have also been greatly studied over the past decade. Recently, many studies have focused on simple fabrication methods for the realization of high aspect ratio structures that maximize the electric edge effect. Such nanostructures have been fabricated on planar platforms (i.e., aligned nanorods),[85,66] on underlying high aspect ratio nanostructures (e.g., nanospheres, nanorods, and etched fiber bundles),[67,86] and as individual nanoparticles in solution (i.e., nanostars).[43,87,60]

In the case of planar substrates, one of the simplest fabrication methods involves physical vapor deposition of aligned nanorods [see Fig. 5(b)] at extreme angles.[85,66] These substrates are fabricated by depositing 200 to 500 nm of silver on glass slides that are rotated at angles greater than 75 deg from the horizontal position.[85] The resulting substrates end up with a series of high aspect ratio nanorods aligned at a 50 to 60 deg angle with respect to the slide.[85] Taking advantage of the lightning rod effect as well as the semiordered, aligned array, these nanostructures offer SERS enhancement factors as high as 5×10^8,[66] with good reproducibility, all using a single-step fabrication process.

The use of sharp edges and high aspect ratio structures has also recently been applied to MeFON substrates.[67] One method recently developed for fabrication of such substrates results in the generation of immobilized silver nanorods assemblies (INRA) on polymeric spheres [see Fig. 5(c)].[67] In this method, silver is deposited via physical vapor deposition on polymer nanospheres while being rapidly spun (~550 rpm). Based on the particular deposition conditions employed (i.e., sphere size and rotation rate), an array of aligned silver nanorods is created. By varying the size of the nanospheres used to make the underlying monolayer, the LSPR can be varied controllably to tune the SP absorption maximum.[67] Employing this method, silver substrates have been generated that can be tuned from 450 to 1100 nm (with nanospheres ranging in size from 320 and 790 nm) while having EF of 10^7 to 10^8.[67]

Another recently developed plasmonic nanostructured array with sharp edges that have demonstrated significant SERS enhancement factors is fabricated by coating tapered and chemically etched fiber optic imaging bundles with metal via physical vapor deposition [see Fig. 5(d)].[86] Employing fiber optic imaging bundles, which are tapered with a micropipette puller and etched with hydrofluoric acid, an array of pyramidal shaped spikes is generated, with each metal-coated spike capable of focusing the electric field on its edges. Additionally, by varying the tapering parameters, the spacing between the individual pyramidal spikes can be altered precisely, controlling interspike electric field interactions. Using such pyramidal nanostructures, silver-coated versions of these substrates have been demonstrated to exhibit SERS enhancement factors as great as 10^9.[79,86]

While fabrication of extended arrays of sharp-edged SERS substrates are useful for many applications, analysis of microscopic and nanoscopic environments (e.g., intracellular) via SERS requires much smaller SERS substrates that do not require aggregation to provide significant enhancement. Recently, sharp-edged, branched SERS nanoparticles known as nanostars [see Fig. 5(e)] have been developed for such analyses.[87] The high anisotropy of these plasmonic nanostructures results in greatly enhanced electric fields in multiple spots on the star's surface due to the lightning rod effect.[43] Furthermore, the optimal plasmon absorption band of these structures is tunable by varying the core diameter to branch length ratio.[87] Employing this nanostar configuration, individual gold nanostars have been demonstrated to possess SERS enhancement factors as large as 4×10^5, which is 2-fold larger than nonstarred silver nanoparticles, while conserving the stability and biocompatibility inherent to the gold.[60]

2.2.3 *Organized structures*

Since hot spots associated with nanogaps between two or more SERS active nanoparticles within a few nanometers of each other are known to generate the largest possible electric fields and corresponding SERS enhancements, the desire to fabricate nanogap arrays with ordered spacings has been a highly active area of research. By generating such ordered arrays, the potential for reproducible and sensitive quantitative SERS analyses exists. In addition to the development of patterned arrays (already described), there has also been a great deal of recent research into the development of isolated SERS active nanoparticle dimers[68,88–91] and target-triggered, ordered nanoparticle aggregates.[69,92–95] Such isolated dimers and ordered aggregates offer the potential of significantly enhanced SERS signals over individual particles or larger ordered arrays, with good reproducibility.

Several different methods have recently been developed for the fabrication of isolated SERS active dimers and organized aggregates. One such method includes asymmetrically functionalizing SERS nanoparticles with thiol linkers that are used to attach to a complementary nanoparticle forming the dimer [see Fig. 5(f)].[88,89] Alternatively, isolated dimeric structures have also recently been fabricated, with a high degree of precision, by a process known as on-wire

lithography [OWL; see Fig. 5(g)]. In OWL, alternating layers of gold nanorods and sacrificial polymer are electrochemically grown to specific lengths in anodic aluminum oxide (AAO) templates. After dissolution of the AAO template, the gold polymer rod is coated with silicon dioxide, and the polymer layer is dissolved, creating a gold dimer of precise dimensions.[90] Because of the precise control over the size and spacing of the linked gold nanoparticles, the SP absorption wavelength can be readily tuned to the desired wavelength for a particular application and EF as great as 10^9 have been reported.[68] Another class of dimer/organized aggregate that has been refined over the past decade has been DNA and RNA origami-based structures [see Fig. 5(h)].[91] Unlike the previous dimer fabrication methods, the oligonucleotide-specific interactions associated with DNA and RNA allow for much more diverse and complicated structures to be formed. However, the complexity of forming such elegant and well-defined nanostructures is limited by the melting and binding conditions required for each different interaction. To provide plasmonic nanostructures, the oligonucleotides are functionalized with colloidal metal nanoparticles at specific locations, providing a means of coordinating the nanoparticles with precision limited only by the flexibility of the specific oligonucleotide sequences employed.[91]

An alternative approach to controlled aggregation of SERS nanoparticles that have recently seen growth for SERS sensing applications has been analyte-induced or analyte-triggered nanoparticle aggregation-based systems [see Fig. 5(i)].[92,93–95] This sensing strategy was first developed as a colorimetric detection platform in which the analyte-induced aggregation resulted in a measurable color change,[96,97] but has since been applied to solution-based oligonucleotide sensing applications via SERS. In the SERS-based version of this technique, two different batches of ssDNA and Raman reporter molecule-bound SERS nanoparticles are fabricated.[92] One batch of these nanoparticles contains an ssDNA sequence complementary to one half of the target/analyte oligonucleotide sequence, and the other batch contains an ssDNA sequence complementary to the other half of the analyte oligonucleotide. When these two batches of labeled nanoparticles are in the presence of the desired analyte sequence, controlled dimers are formed resulting in a greatly enhanced Raman signal from the reporter molecules on the nanoparticles' surface.[92] Similarly, aptamers have also recently been employed as the analyte-targeting sequence responsible for nanoparticle dimerization, allowing for this concept of analyte-induced aggregation to be expanded beyond DNA and RNA sensing applications to other target species such as proteins.[94]

Even more recently, the possibility of using hydrodynamic forces to trap analyte molecules in a SERS active nanogap has been demonstrated.[69] In this work, SERS active nanostructures, known as nanofingers [see Fig. 5(j)], trap the analyte of interest in a highly SERS active environment for detection. These nanofinger traps consist of an array of polymeric flexible nanorods whose extremities are coated with metal.[69] These nanofingers are exposed to a solution containing the analyte of interest and are then allowed to dry. As the sample dries, the rods bend due to the capillary forces experienced during evaporation and form aggregates around the few molecules left in the nanogap, providing a highly aggregated SERS substrate with large EF.[69]

3 Surface Plasmon Resonance Sensing

Another spectroscopic sensing technique that relies heavily on plasmonic materials and has seen significant advances with the introduction of enhanced plasmonic nanostructures is SPR sensing. SP resonance was first observed in 1968 using a prism in contact with a pair of quartz slides that had a 100-nm thick silver film deposited between them as the plasmonic material.[98] Since this initial observation and the development of the associated theory,[98,99] the field of SPR sensing has seen significant application to many fields due to its relatively noninvasive and localized probing of the sample. In short, SPR sensing is a technique that utilizes the evanescent field of an SP propagated across a metallic surface to detect changes in the dielectric constant of the sample directly in contact with the plasmonic material (or within a few nanometers). As this evanescent field interacts with the analyte, the resulting change in light intensity or shift in transmitted excitation light wavelength or angle is directly related to changes in the refractive index of the sample (see Fig. 7).[100,101] This change in transmitted light properties (i.e., intensity, wavelength, or angle) allows for the noninvasive detection of chemical or biochemical species of interest. In addition, by modifying the plasmonic surface with receptors, specific and sensitive SPR sensors can be fabricated.

3.1 *Traditional Surface Plasmon Resonance Nanostructures*

Despite the widespread applicability and universal detection capabilities of SPR, the somewhat bulky and inflexible grating-based [see Fig. 8(a)] and prism-based [see Fig. 8(b)] optical systems limited its application somewhat in the early years. However, with the advent of optical fibers in the 1980s and 1990s, the potential applicability of SPR to many new sample environments became apparent. For instance, biological environments that were previously unsuitable for

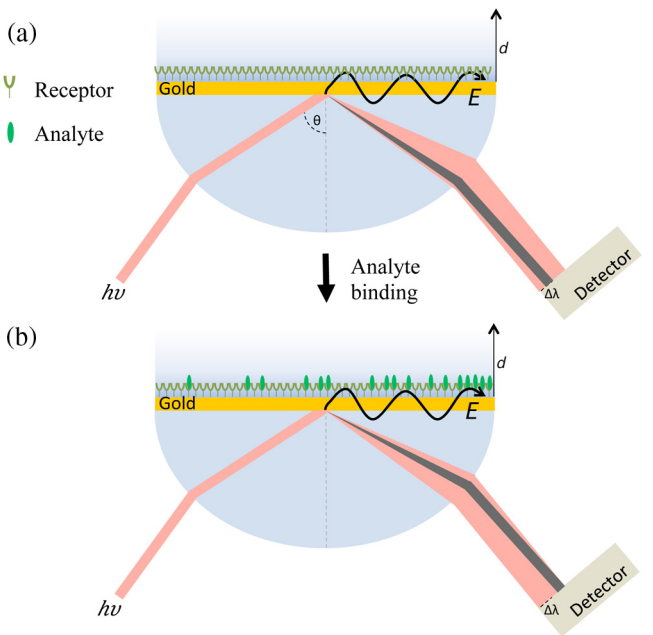

Fig. 7 Schematic depiction of SPR measurement using Kretschmann configuration: (a) before analyte is present and (b) after analyte is present, showing a spectral shift at the detector.

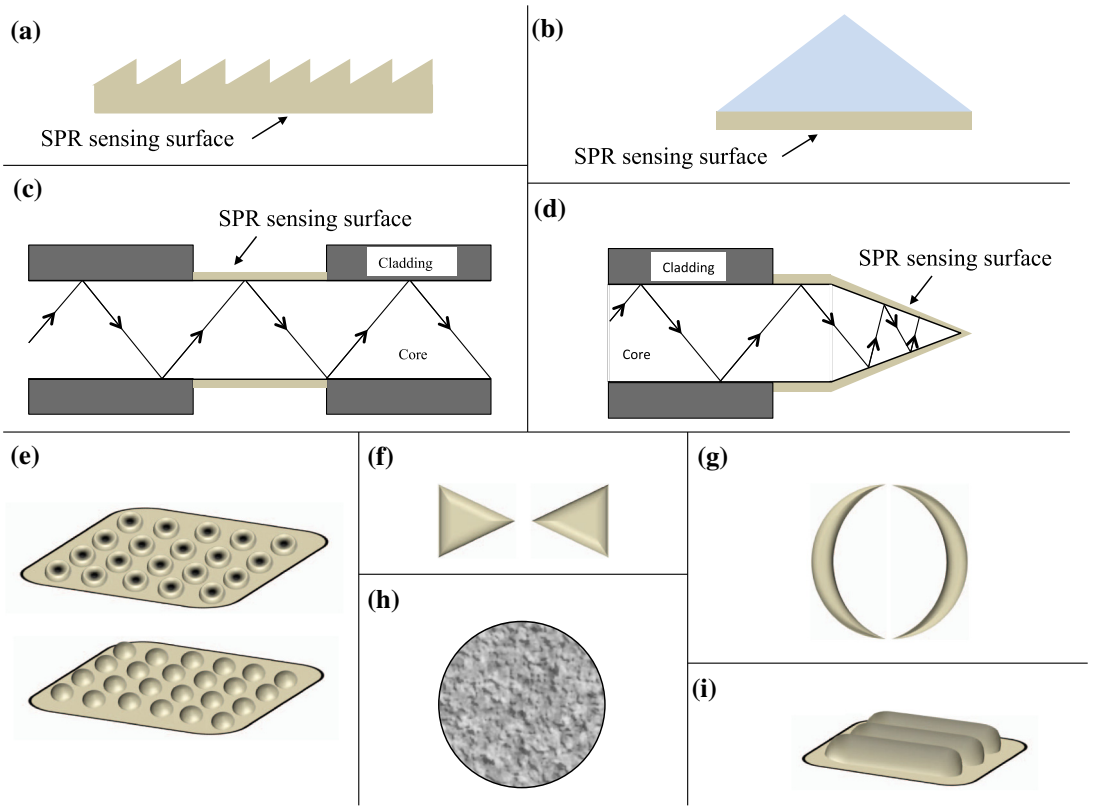

Fig. 8 Schematic images depicting both traditional and recent plasmonic nanostructures employed for SPR sensing, including (a) gratings, (b) prisms, (c) fiber optics, (d) tapered fibers, (e) nanodot and nanohole arrays, (f) nanotriangles, (g) nanocrescents, (h) nanoporous disks, and (i) nanowires.

SPR sensing due to size restrictions were now possible due to the flexibility and durability of the optical fibers.[102–104] The earliest of these fiber optic SPR sensors were fabricated by removing the cladding material from a portion of the optical fiber and depositing a thin film of metal directly on the core of the fiber in that area [see Fig. 8(c)]. Once exposed to the sample, changes in the refractive index of the sample resulted in differences in the intensity of the light transmitted through the fiber.[105] Since the wavelength of optimal plasmon excitation (and thus evanescent excitation) in SPR is dependent on the physical properties of the metal employed as well as the amount and geometry of the metal, tapered optical fibers [see Fig. 8(d)] with different amounts of metal have been investigated as early as the late 1990s for tuning the optimal excitation light, thereby increasing the SPR sensitivity.[106] Most recently, nanoscale alterations to plasmonic surfaces on which the evanescent wave is propagated and the introduction of plasmonic nanoparticles for enhanced sensitivity have significantly expanded the number of different types of SPR sensing platforms that exist, further increasing the potential applications for SPR. The next portion of the review will focus on recent advances to SPR sensing associated with these various nanostructured plasmonic geometries.

3.2 *Recent Advances in Surface Plasmon Resonance Nanostructures for Sensing*

Recent advances in SPR sensing associated with plasmonic nanostructures have largely revolved around the introduction of nanostructured metallic surfaces for enhanced sensitivity and tunability of the SPR probes. This section discusses the most recent advances associated with the introduction of plasmonic nanostructures to SPR sensing platforms and their significance. Table 2 shows the influence of plasmonic nanostructure shape and size on SP energies and SPR sensitivity. This table allows for the comparison of the effect of metal nanostructure size and periodicity on the plasmon absorption behavior as well as SPR sensitivity. As can be seen from this table, trends described in the following sections (e.g., increasing particle size red shifting absorption maxima) are demonstrated and quantified (when possible). In addition, specific dimensions can be easily associated with optimal optical properties.

One of the most recent advances in SPR sensing has been the introduction of nanostructured nanoparticle arrays on the sensing tips of fiber optic SPR probes. Introduction of plasmonic nanostructures onto SPR surfaces results in the introduction of LSPRs that can be easily tuned to provide significant increases in sensitivity, due to the ability to match the LSPR to the desired wavelength for a particular analysis.[109] In an early example of nanoparticle-coupled fiber optic SPR, an array of 85-nm diameter silver nanodots was fabricated on the tip of a fiber with a periodicity of 400 nm. Figure 8(e) depicts an example of such a nanodot array. The resulting probe exhibited an LSPR of 656 nm that resulted in sensitivities capable of monitoring biological samples with pM limits of detection.[109] Coupling such nanostructured arrays on optical fibers in which Bragg diffraction gratings have been generated can further increase the applications of these sensitive SPR

Table 2 Properties of plasmonic structures for SPR.

Triangle arrays						
Metal	Array type	Length (nm)	Periodicity (μm)	λ_{SPR} (nm)	Sensitivity ($\delta\lambda$/RIU)	References
Au	Triangle	2000	3.2	500 to 600	1065	107
		1000	1.5	500 to 600	849	107
		750	1	500 to 600	796	107
		475	0.82	500 to 600	770	107
		275	0.65	500 to 600	769	107
Micro- and nanohole/nanodot arrays						
Metal	Array type	Diameter (nm)	Periodicity (μm)	λ_{SPR} (nm)	Sensitivity ($\delta\lambda$/RIU)	References
Au	Microhole	1856	3.2	500 to 600	4238	107
	Microhole	1536	3.2	500 to 600	3325	107
	Nanohole	896	3.2	500 to 600	3253	107
	Nanohole	448	3.2	500 to 600	3281	107
	Nanohole	855	1.5	500 to 600	4244	107
	Nanohole	645	1.5	500 to 600	3046	107
	Nanohole	540	1.5	500 to 600	2924	107
	Nanohole	450	1.5	500 to 600	2744	107
	Nanohole	600	1	500 to 600	3681	107
	Nanohole	470	1	500 to 600	3357	107
	Nanohole	290	1	500 to 600	2826	107
	Nanohole	250	1	500 to 600	3050	107
	Nanohole	500	0.82	720	—	108
	Nanohole	352.6	0.82	500 to 600	2929	107
	Nanohole	287	0.82	500 to 600	3398	107
	Nanohole	180.4	0.82	500 to 600	3091	107
	Nanohole	253.5	0.65	500 to 600	4217	107
	Nanohole	169	0.65	500 to 600	4145	107
	Nanodot	85	0.4	656	—	109
	Nanohole	90	0.2	500 to 600	—	110
Nanoslits						
Metal	Array type	Slit size (nm)	Periodicity (nm)	λ_{SPR} (nm)	Sensitivity ($\delta\lambda$/RIU)	References
Ag	Nanoslit	45	450	~460 to 540	~500	111
Nanocrescents						
Metal	Crescent type	Width (nm)	Periodicity (nm)	λ_{SPR} (nm)	Sensitivity ($\delta\lambda$/RIU)	References
Au	Opposing	~200 to 450	—	~1400 to 2200	—	112
	Stacked	~100	~500	1484	—	113
	Stacked	~100	~500	2210	—	113

Table 2 (*Continued*).

Nanoporous disks						
Metal	SPR type	Diameter (nm)	Pore size (nm)	$\lambda_{max,SPR}$	Sensitivity ($\delta\lambda$/RIU)	References
Au	Longitudinal	300	8.5	958	—	114
		300	11.2	990	—	114
		300	13.8	906	—	115
		400	13.7	1100	125.3	115
		500	12.5	1300	—	115
		700	12.8	1806	—	115

probes by allowing for the multiplexed detection of several different analytes simultaneously.[116]

In addition to fiber-optic-based SPR sensing, introduction of arrays of plasmonic nanostructures to other SPR sensing platforms has also grown dramatically in recent years. Among the most commonly employed SPR platforms in which nanoparticle arrays have been introduced are SPR sensors that operate in the Kretschmann configuration (see Fig. 7). Using the Kretschmann configuration, the nanostructure arrays can either be fabricated on or within the metallic film (typically gold) used for SP propagation, allowing for coupling of the SP associated with the metallic film with the LSPR associated with the nanostructured array. Adapted from early SPR sensing platforms that employed gratings, one such example of nanostructures in metallic films is nanoslits or dual-sided nanoslits.[111,117] Similar to the previous grating structures, multiple plasmons can be supported, with the nanostructure providing LSPRs from the ultraviolet to the NIR, while also exhibiting enhanced transmission. An alternative nanostructure to these nanoslits that have also recently been demonstrated to provide enhanced SPR due to strong LSPRs is nanohole arrays [see Fig. 8(e)]. Using such nanohole arrays etched into a gold metallic film, it has been shown that the LSPR can be easily tuned through the visible and NIR region of the electromagnetic spectrum simply by altering the interhole separation distance.[110,108] This tunability for a particular application of interest allows for dramatic increases in SPR sensitivity.[107,118–120] Although the tunability of such nanoarrays in gold is limited to the NIR and longer wavelength region of the visible (i.e., ~500 nm or greater), a variation of these nanoslit and nanohole arrays, known as nanotriangle arrays [see Fig. 8(f)],[107] has demonstrated the ability to further expand the range of LSPR wavelengths achievable simply by altering the structure. This demonstrates the vast potential of various nanostructures for enhanced SPR sensing.

As has been previously described for SERS, not only does the size and material composition of the metallic nanostructure influence the LSPR wavelength, but so does the nanoparticle's shape. To demonstrate the significance that a nanoparticle's shape can have on SPR sensing (via the LSPR) as well as optimize the local electric field experienced at particular locations, Vogel et al. have employed stacked nanocrescent structures to allow for LSPR tuning through the NIR region of the electromagnetic spectrum.[113] These nanocrescent structures [see Fig. 8(g)] are simply fabricated by angled deposition of metals via physical vapor deposition on ordered nanosphere arrays, in a fashion similar to that described previously for MeFON SERS substrate fabrication.[112,113] After the nanocrescents have been fabricated, the underlying nanospheres are removed, leaving only the metallic nanocrescent behind. Using these metal nanocrescents as the plasmonic structure, it is possible to tune the LSPR simply by altering the width of the crescent as well as the contour angle. Furthermore, alignment of these crescents across the substrate allows for generation of a propagating SP as well as the LSPR at the crescent tips,[113] making such structures extremely sensitive and flexible for many SPR sensing applications.

Another recently developed method for providing easily tunable nanostructured arrays for SPR sensing is the use of nanoporous gold disks [see Fig. 8(h)] that can be dealloyed to provide variations in pore size and shape, resulting in highly tunable shifts in the optimal SPR wavelength.[114,115,121] Using such nanoporous gold disks, it has been demonstrated that the significantly increased surface area associated with the nanostructured surfaces, along with the ability to attach various receptors, allows for greatly enhanced sensitivity over planar SPR sensing platforms.[121] In addition, since these disks have both a diameter as well as a depth associated with them, both longitudinal and transverse plasmon absorption bands exist, providing two potential plasmon absorption bands that can be tuned for a particular application.[121]

An alternative means of introducing plasmonic nanoparticles to SPR sensing platforms that have recently been demonstrated to provide dramatically enhanced SPR sensitivities as well as reduced surface fouling has been the incorporation of metallic nanowires and nanoparticles in thin polymer coatings.[122] Using this fabrication method, the distance between the SP-propagating metal surface and the plasmonic nanoparticles can be controlled to allow for alteration of the SP and LSPR coupling.[122] As with the inclusion of metallic nanostructures with other previously described SPR sensing platforms, the separate controlled tunability of the LSPR and SP allows for extension of the spectral range over which such platforms can sensitively operate. Furthermore, immobilization of metallic nanowires in the polymer coating provides plasmonic nanostructures that can result in intense electric fields due to the lightning rod effect, as well as be aligned to provide coupling and corresponding increases in sensitivity due to LSPR tuning.[122]

4 Metal-Enhanced Fluorescence

MEF (also referred to as surface-enhanced fluorescence, plasmon-enhanced fluorescence, and radiative decay engineering) represents another plasmonically enhanced sensing technology that has seen significant advances in recent years due to the incorporation of plasmonic nanostructures. As with SERS, MEF was first described in the 1970s[123–125] and provides an increased emission of characteristic electromagnetic radiation from an analyte that is in proximity to a plasmonic nanostructured surface.[123,125,126–130] While the overall result of increased optical emission/scattering is the same for both SERS and MEF, the underlying phenomenon is very different for these two plasmonically enhanced sensing techniques.

MEF arises from a dipole interaction between a fluorophore and an LSP. As seen in Fig. 9, incoming radiation interacts with both the metal surface and the fluorophore. This produces an enhanced luminescence that can be observed. This enhancement is primarily due to a dipole interaction of the fluorophore with the plasmonic nanostructured surface, providing a rapid energy transfer pathway from the fluorophore to the metal (and vice versa) and a subsequent radiative emission from both the metal and the fluorophore.[126,127,129] Because of the rapid energy transfer between the fluorophore to the plasmonic nanostructure, other nonradiative relaxation pathways are reduced, resulting in an overall increase in fluorescent emission. For this reason, MEF works best (i.e., greatest enhancement of luminescence) for fluorophores that typically exhibit low-quantum yields, whereas high-quantum yield fluorophores typically exhibit less enhancement.[131]

Unlike SERS and SPR, in which the closer the analyte molecule is to the plasmonic surface the greater the signal, MEF requires that the fluorophore be located at an optimal distance away from the metal's surface, typically somewhere between 10 and 20 nm depending on the specific analyte and plasmonic nanostructure.[127,129,132,133] At distances that are too short, the fluorescence of the analyte is quenched, and at distances too far, the dipole coupling between the fluorophore and the plasmonic nanoparticle is too weak to enhance the fluorescence. A schematic depicting why an optimal distance exists for MEF is shown in Fig. 10, with the highest enhancement occurring at a specific distance due to the competing processes. Although the model data in Fig. 10 show a maximum enhancement at a distance of approximately

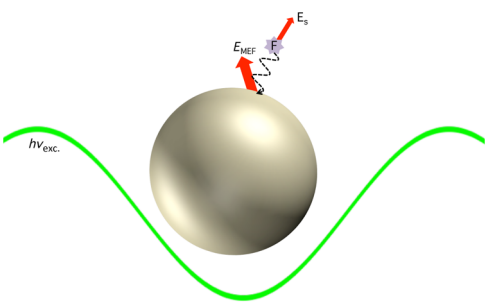

Fig. 9 Schematic diagram depicting MEF, where energy transfer between the fluorophore near a plasmonic surface can rapidly transfer energy, resulting in enhanced fluorescence, emitted both from the fluorophore and the metallic surface.

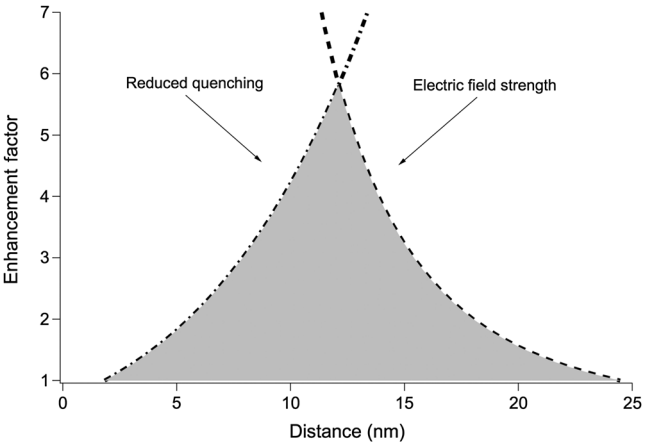

Fig. 10 Schematic diagram depicting the fluorophore-metal distance-dependence of the MEF enhancement and the competing processes (quenching and local electric field strength) involved. The particular model shown is based on 6-carboxy fluorescein and an 89-nm diameter silver nanoparticle.[132]

12 nm for this particular system, the exact position of the maximum MEF enhancement shifts slightly based on the specific plasmonic structure (electric field produced) as well as the fluorophore coupling to it. Once a fluorophore is within the optimal distance for an MEF interaction to occur, there must also be a spectral overlap between the plasmon absorption band of the nanoparticle and fluorescence excitation band of the fluorophore in order for efficient energy transfer to occur.[134–136] The resulting energy transfer between the fluorophore and the metal not only increases the intensity of the fluorescent light but also decreases the fluorescence lifetime of the analyte, thereby increasing its photostability.[126, 127, 129,131,137,138]

4.1 *Traditional Metal-Enhanced Fluorescence Nanostructures for Sensing*

The first application of MEF for sensing involved the use of silver island films on glass slides, with very slight enhancements being realized.[139,140] Since this time, MEF has experienced a strong growth in biosensing and bioimaging applications,[130,141–147] with silver island films remaining the most commonly employed plasmonic nanostructures due to their ability to provide relatively short wavelength visible plasmon absorption bands for small island sizes. Additionally, colloidal silver and gold nanoparticles have also seen significant use over the years for particular applications, where free-floating nanostructures are required (e.g., cellular imaging),[148,149–151] or in filter paper-based MEF substrates that can be used for rapid disposable sample analyses.[152]

In addition to the traditional silver island films and colloidal nanoparticles used for MEF, several other plasmonic nanoparticles have also been developed over the past several decades to provide greater signal enhancements. Among the most notable of these are nanotriangle arrays or bowties[151,153,154] and silver fractals (fabricated via electrochemical growth).[155] In each of these cases, the resulting plasmonic nanostructures resulted in significantly greater MEF enhancements than silver island films for the particular fluorophores employed.

4.2 *Recent Advances in Metal-Enhanced Fluorescence Nanostructures for Sensing*

Due to the need for strong spectral overlap between the fluorescence excitation band of the analyte and the plasmon absorption band of the metallic nanoparticle involved in MEF analyses, many of the advances in plasmonic nanostructures used for MEF sensing over the past 5 years have involved the development and application of nanostructures capable of extending the spectral range over which such analyses can be performed. Unlike SERS analyses, which can be performed at any wavelength, a plasmonic nanostructure can be tuned to the fluorescence excitation bands for fluorophores that occur at a specific wavelength ranging from the ultraviolet to the NIR. For this reason, many of the recent advances in MEF involve developing plasmonic nanostructures capable of having their plasmon absorption bands tuned over large spectral ranges through the use of various structures and mixed materials as well as providing optimal interaction distances between the fluorophore and nanoparticle. Although a great deal of recent research in the field of MEF has revolved around sensor development aspects such as integration of receptors with the MEF-enhancing nanostructures for specificity, this section of the review will focus specifically on the recent advances in plasmonic nanostructures for MEF.

A summary of the various MEF plasmonic nanostructures and their optical properties is provided in Table 3. This table highlights the relationship and trends between material, size, and structure of the various MEF nanostructures and their optimal plasmon absorption wavelengths as well as sensitivities. These values were compiled from the literature and when not explicitly quantified, they were estimated from data in the papers. As can be easily seen from this table, a clear relationship between optimal LSPR and fluorophore excitation maximum exists for optimal enhancement. Furthermore, the various structures tabulated are referenced for easy access to detailed fabrication parameters.

4.2.1 *Individual nanoparticle substrates*

Core–shell nanoparticles have become increasingly employed in MEF over the past decade. Unlike core–shell nanoparticles employed for SERS analyses, however, the core and shell materials in MEF are often reversed, with the core being composed of a plasmonic metal and the outer shell corresponding to a dielectric material such as silicon dioxide. By fabricating core-shell nanoparticles in this fashion, the dielectric shell provides a built-in spacer for optimal positioning of the fluorophore, while the inner metallic core can be tuned via size to have an optimal plasmon absorption wavelength for the fluorophore of interest [see Figs. 11(a) and 11(b)]. One of the more recent advances in the fabrication of such core–shell nanoparticles has been the development of a simplified one-pot synthesis method for the fabrication of silver/graphene core nanoparticles coated with a SiO_2 shell.[171] Using these nanoparticles and doping fluorescein isothiocyanate (FITC) into the shell, MEF enhancements of 3-fold were obtained despite the minimal overlap between the plasmon absorption band and the fluorescence excitation band, suggesting that such one-pot syntheses as these, once optimized, can provide a simple and rapid fabrication method for highly sensitive MEF probes.

Another recent advance in core–shell nanoparticle structures for MEF has been in the fabrication of silver nanoparticle cores surrounded by polyelectrolyte shells.[172] Unlike conventional solid-shell materials used to fabricate core–shell nanoparticles, the polyelectrolytes provide a tunable film that can be easily manipulated to tune the optimal fluorophore nanoparticle distance for the particular fluorophore-nanoparticle combination employed. Using these polyelectrolyte shells surrounding silver nanoparticle cores, some of the largest MEF enhancements to date have been measured (i.e., 3.7- to 6.2-fold), offering a potentially widely applicable new plasmonic nanostructure for numerous MEF applications.

In addition to chemical sensing applications, MEF has also become a significant tool for bioimaging applications. To avoid complications associated with autofluorescence backgrounds resulting from ultraviolet and visible excitation of biological samples, it is often desirable to perform MEF bioimaging in the NIR region of the spectrum. To this end, Cheng et al. have developed MEF core–shell nanoparticles that consist of a gold core surrounded by a silicon dioxide shell doped with AgS.[173] Due to the strong coupling of the Au cores to the AgS, the resulting MEF enhancement factor was found to be as large as 28-fold, providing an extremely enhanced signal with NIR emission ideal for tissue imaging.

As with SERS, the use of nanorod-based plasmonic nanostructures for MEF has seen a significant increase in the past 5 years due to their ability to exhibit two different independent plasmon absorption bands associated with the transverse and longitudinal plasmons supported on the surface.[168,170,174] Using such structures, and the two distinct plasmon absorption bands simultaneously supported by them, multiplexed analyses can be performed. In one such example, simultaneous SERS and MEF detection using a single nanorod was demonstrated, with the longer wavelength longitudinal mode providing the SERS enhancement and the shorter wavelength transverse mode enhancing the MEF.[169] Furthermore, core–shell-type structures of mesoporous SiO_2 around gold nanorods have also recently been produced, demonstrating the distance tunability associated with the fluorophore nanoparticle distance as well as the spectral tunability of the nanorod plasmon absorption.[174,167]

4.2.2 *Ordered nanostructures and patterned arrays*

Another category of MEF plasmonic nanostructures that have seen a significant growth over the past 5 to 10 years has been the development and application of ordered (or patterned) arrays of nanostructures. The uniformity and regular pattern of such structures offers many advantages, including the ability to perform multiplexed analyses, as well as improved reproducibility and sensitivity in some cases. One such class of plasmonic nanostructured arrays that have recently been employed is periodic gratings and grating-like structures.[175] In these structures, the lines etched into the metal surface provide the controlled nanostructure and allow for a large range of plasmon resonances to be generated. This large range in turn results in a single MEF platform capable of being applied to a large number of different fluorophores.[157]

Related to nanohole arrays [see Fig. 8(e)] described in plasmonic nanostructures employed in SPR, nanoapertures and nanoaperture arrays have also seen recent application

Table 3 Properties of plasmonic nanostructures for MEF.

Arrays

Metal	Array type	Nanopore/ nanoparticle size (nm)	Periodicity (nm)	EF	Fluorophore	λ_{LSPR} (nm)	Fluorescence excitation max (nm)	References
Au	Nanoporous	38	Random	—	QD	~500	525	156
	Nanoporous	51	Random	—	QD	~650	605	156
	Grating	—	600	13	QD	500 to 600	600	157
	Nanohole	140	440		Alexa647	660	650	158
	Nanoaperture	135	440	120	Alexa647	—	650	159
	Antenna in-a box	290 × 100 × 76 (box) 50 (particle dia)	—	1100	Alexa647	740	650	160
Ag	Nanotriangles	300	Monolayer	7.8	Alexa488	495	495	161
	Nanotriangles	500	Monolayer	5.7	Alexa680	680	679	161
	Nanotriangles	650	Monolayer	10	Alexa750	750	749	161
	Nanocone	500 × 180	280	30	Rhodamine 6G	320	528	162
Ag/Au	Nanocomposite	Varies	Random	15	ATTO655	—	663	163
AAO	Nanopore	10	—	100	Rhodamine 6G, fluorescein	—	528, 460	164
	Nanopore	60	~20 nm	50 to 200	Rhodamine B	390 to 670	528	165
Cu	MeFON	130	~130	13.7	5,10,15,20-tetrakis (4-carboxyphenyl) porphyrin (TCCP)	—	650	166
	MeFON	355	~355	69.3	TCCP	630	650	166
	MeFON	462	~462	89.2	TCCP	675	650	166
	MeFON	534	~534	37.2	TCCP	715	650	166

Nanorods

Metal	—	Aspect ratio (uncertainties)	—	EF	Fluorophore	λ_{LSPR} (nm)	Fluorescence excitation Max (nm)	References
Au	—	2.5 (0.5)	—	2.5	Doxorubicin HCl	510, 731	590	167
	—	2.7	—	~2.2	Rose Bengal	513, 676	549	168 and 169
	—	2.9 (1)	—	2.4	Doxorubicin HCl	510, 746	590	167
	—	3.4	—	~2.2	Rose Bengal	513, 746	549	168 and 169
	—	3.8	—	~2.2	Rose Bengal	513, 780	549	168 and 169
	—	3.8 (1)	—	2.1	Doxorubicin HCl	510, 786	590	167
	—	4	—	~2.2	Rose Bengal	513, 805	549	168 and 169
	—	4 (0.5)	—	2.1	Doxorubicin HCl	510, 821	590	167
	—	4.2	—	~2.2	Rose Bengal	513, 851	549	168 and 169
	—	4.2 (0.5)	—	2.5	Doxorubicin HCl	510, 843	590	167
	—	4.6 (1)	—	2.2	Doxorubicin HCl	510, 891	590	167

Table 3 (*Continued*).

Ag	—	2.1 (~0.8)	—	~1.0	FITC	428	492	170
	—	4.3 (~0.8)	—	~0.9	FITC	510	492	170
	—	7.6 (~1.5)	—	~2.2	FITC	n/a	492	170
	—	11.8 (~2.2)	—	3.7	FITC	378	492	170
	—	12.6 (~5.1)	—	~3.0	FITC	378	492	170

Core–shell

Core material	Shell material	Diameter (nm)	—	EF	Fluorophore	λ_{LSPR} (nm)	Fluorescence excitation Max (nm)	References
Ag-graphene	SiO_2	60	—	3	FITC	395	492	171
Ag	PEI/HA	43.8	—	3.7 to 6.2	IgG-modified CdSe/ZnS quantum dots	—	—	172
Au	SiO_2/Ag_2S	57	—	28	Ag_2S	524	665	173

to MEF sensing. Due to the inherent sensitivity of fluorescence spectroscopy as well as the further enhancement capabilities of MEF, MEF has seen significant interest for single-molecule sensing applications. Employing nanoapertures as the plasmonically active nanostructure for such studies, not only provides a tunable plasmon absorption, dependent on the size of the aperture, but also a directionality to the resulting fluorescence emission determined by the conical angle of the aperture. This has recently been demonstrated to remove the need for high numerical aperture objectives in experimental systems for single-molecule detection via MEF.[159,158] Unfortunately, the directionality of the signal comes at the cost of reduced signal due to transmission through the aperture as well as restricting the optical geometry of the measurement system by making it a transmission geometry. More recently, an alternative plasmonic

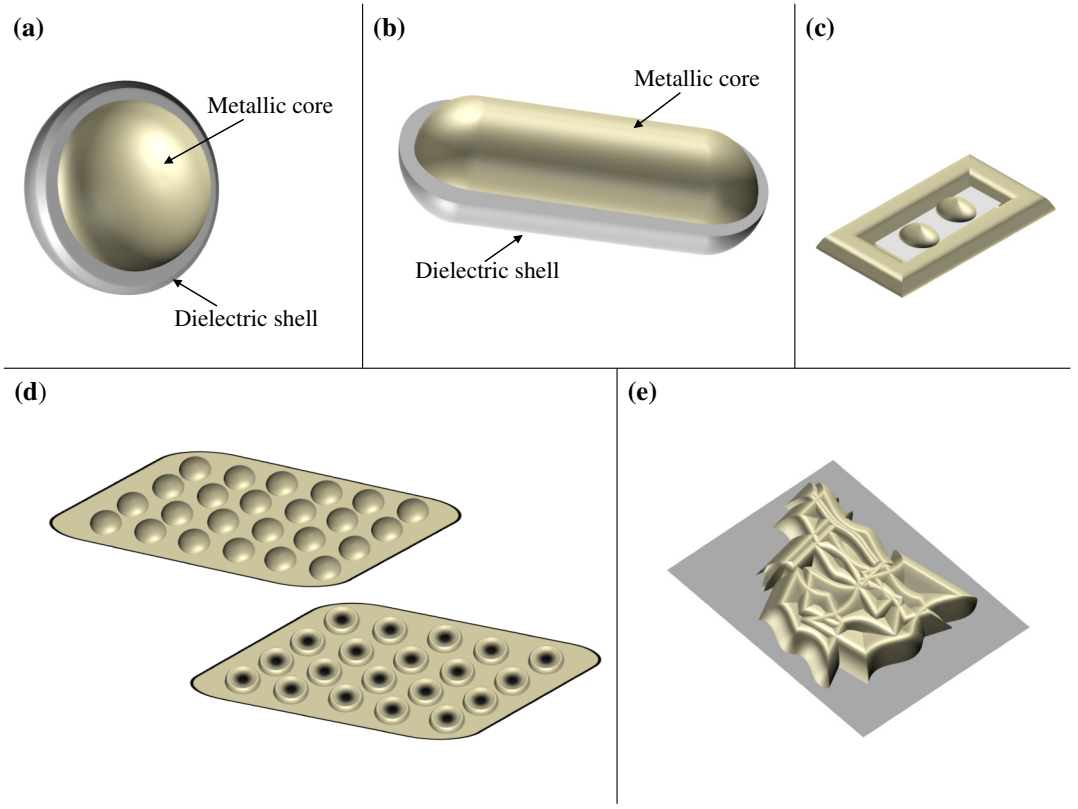

Fig. 11 Schematic images depicting recent plasmonic nanostructures developed for MEF sensing, including (a) core–shell nanoparticles, (b) nanorods, (c) antenna in a box, (d) nanodot and nanohole arrays, and (e) wrinkled arrays.

nanostructure with a related design, known as an "antenna in a box" [see Fig. 11(c)], has been developed for single-molecule MEF measurements via a backscatter geometry. These nanostructures are created by milling a rectangular well into a gold film and inside of the approximately 250-nm long box, leaving two semispherical gold nanoparticles to act as a dimer pair. The resulting intense electric field generated at the hot spot between the two nanospheres results in large MEF enhancement factors and the surrounding box provides an efficient reflector for backscatter collection of the signal.[160,156] By changing the nominal diameter of the nanosphere dimer particles, the optimal plasmon absorption wavelength can be easily changed to match a particular fluorophore. Arraying such a nanoantenna in boxes across a substrate can allow for rapid multiplexed analyses of many samples with single-molecule detection sensitivities.[160,156]

Another form of nanohole/nanopore array [see Fig. 11(d)] that has recently been employed for MEF sensing applications involves the use of AAO arrays, in which nanoholes bored in the AAO material provide the nanostructured surface for plasmon oscillation as well as pores for potential incorporation into microfluidic devices.[176,164] By using aluminum as the plasmonic material, it is possible to directly generate SPs in the AAO that exhibits much shorter wavelength plasmon absorption bands than other commonly employed metals. In addition, the low cost of the materials as compared to coinage metal-based MEF substrates potentially allows for disposable MEF sensing platforms that are capable of exciting fluorophores with absorption bands in the difficult-to-access blue to UV region of the electromagnetic spectrum. Furthermore, due to the distance-dependence of MEF, the native oxide layer that dramatically reduces the usefulness of aluminum substrates for SERS and SPR analyses does not significantly degrade the MEF enhancement factors. Using these same inexpensive AAO surfaces, and filling the pores with various other metals to generate metallic nanowells instead of the pores, several different groups have been able to shift the optimal plasmon absorption band from the UV through the NIR. For instance, by generating silver nanowells through physical vapor deposition of silver on the underlying AAO nanopore structures, MEF substrates with significantly red-shifted (i.e., NIR absorbing) plasmons have been demonstrated,[165] while incorporation of platinum can support short wavelength plasmon resonances while also providing additional stability to the structure.[177]

Patterned deposition processes such as NSL and related variations have also been successfully used recently to generate highly enhancing ordered arrays capable of focusing the electric field from the SP to particular "hot spots." One recent example of nanosphere lithographically produced MEF nanostructures has been coined "bowties" (similar to nanotriangles in SPR) and was recently demonstrated by Kinkhabwala et al. to provide a highly focused electric field at the location between the tips of adjacent triangles and correspondingly large MEF enhancement factors.[178] In another example, Xie et al.[161] generated a patterned array of silver nanoparticles via NSL that was capable of significantly enhancing the luminescent emission from high-quantum yield quantum dots due to the intense field at the focused "hot spot." Using these focused bowtie nanostructures, the ability to perform multiplexed analyses has also been demonstrated recently simply by altering the dimensions of the individual triangles in the bowtie structure to make them asymmetric,[179] with the length of the triangles defining the LSPR. This asymmetry allows for the simultaneous support of two plasmons of different energies while retaining the sharp edges of the individual triangles for electric field focusing. Although the magnitude of the electric field in between the two triangles is no longer as strong as it is with symmetric triangles, the MEF enhancement factors for such asymmetric bowties are still large enough for many applications.

In addition to the templated deposition of metallic nanostructures onto planar surfaces such as NSL, plasmonic arrays for MEF sensing have also been generated by vapor-depositing plasmonic metals on various types of underlying nanostructures. In addition to the previously discussed nanowell arrays generated by depositing metal films on AAO nanopore arrays, many other nanostructured surfaces have been employed with various metals to provide specific advantages for particular MEF analyses. These advantages range from increasing the biocompatibility of the surface by employing less toxic metals, such as gold, for contact with the sample to providing unique structural designs for enhanced sensitivity, surface area, or plasmon tunability. Although it does not represent a specific MEF-enhancing nanostructure, one recent significant advance in plasmonic structures for MEF sensing has involved the demonstration of an inexpensive one-step galvano approach to depositing thin gold films on contiguous underlying silver sheets or structures.[180] The significance of this work lies in the fact that many traditional silver MEF nanostructured architectures that have exhibited significant MEF enhancement factors can easily be overcoated with conforming thin layers of gold without disturbing the structural features responsible for their MEF enhancements.

While many different MeFON plasmonic nanostructures have been developed for various plasmonically enhanced sensing techniques over the past two decades (many of which have been discussed previously in this review), one particular array structure that was recently developed and has demonstrated significant enhancements for both MEF as well as SERS is known as black silver nanocone arrays.[162] Unlike many other MeFON substrates whose periodicity or nanostructure strongly supports a single or group of plasmon resonances, these black silver arrays take advantage of the extreme broadband absorption provided by silicon nanorod arrays on a planar surface. By coating these underlying irregular silica nanorod arrays with silver, plasmonic surfaces with little to no reflectance are generated, resulting in a plasmonic surface capable of being excited with almost any wavelength light across the visible and NIR spectrum. This intense broadband absorption by the plasmonic nanostructures not only provides the potential for generation of greater magnitude SPs (which result in greater EF) but also provides spectral overlap with a wide variety of fluorophores, making it a universal MEF substrate. Furthermore, the fabrication process for these black silver surfaces is highly scalable.

Another recently developed class of plasmonic array that shows a great deal of promise for MEF sensing applications is wrinkled arrays [see Fig. 11(e)].[181] These highly enhancing MEF arrays are randomly oriented extended surfaces composed of two dissimilar metals (e.g., nickel and gold)

that are shaped through repeated heating and cooling cycles.[182] Due to the different thermal expansion coefficients of the materials, the repeated heating and cooling generate a disordered, wrinkled surface with large areas of intense electric fields following plasmon generation. Using these wrinkled substrates, MEF enhancements as great as 120-fold have been reported.[181] Although the exact mechanism for these extreme enhancements is still unknown, it has been shown that the enhancements are uniform across the surface and not associated with particular "hot spots," suggesting that large areas can be probed with uniform signal enhancement.[181,182] Furthermore, the fabrication technique is inexpensive, manufacturable, and scalable, making these plasmonic nanostructured surfaces a promising platform for MEF sensing.

4.2.3 *Environmentally responsive metal-enhanced fluorescence plasmonic nanostructures*

A recent variation on the wrinkled array theme for MEF substrates has been the generation of MEF structures that vary in enhancement factor depending on local environmental conditions. While many different types have been developed over the past decade,[183–185] they generally function based on the same principle. Typically plasmonic nanostructures (e.g., colloidal nanoparticles and core–shell particles) are embedded in a thermally responsive polymer[183,184] or gel.[185] As the temperature changes, thermal contraction or expansion (associated with cooling and heating) alters the distance between the isolated metallic nanoparticles and the fluorophore, dramatically altering the MEF enhancement factor. To provide temperature-sensitive tunability to these MEF sensing platforms, various combinations of copolymers can be employed.[183]

5 Conclusions

Although the concept of SPs has been theorized since the middle of the last century, recent advances in both theory and experimental design of plasmonic materials for various chemical sensing platforms have resulted in an explosion of knowledge over the past two decades. Advances in both understanding of plasmonic behavior at interfaces and as well as the ability to predictably manipulate the associated electric fields of these plasmons has resulted in entirely new paradigms for chemical sensing. With the significant efforts being put forth in the overlapping areas of SERS, SPR, and MEF sensing as well as the related fields of plasmonic energy harvesting and plasmonic device development, the potential for even greater advances in plasmonics over the coming years is promising.

Acknowledgments

The authors would like to gratefully acknowledge the support of this work by the Eli Lilly Corporation as well as UMBC.

References

1. G. Binnig, C. F. Quate, and C. Gerber, "Atomic force microscope," *Phys. Rev. Lett.* **56**(9), 930–933 (1986).
2. J. E. Demuth et al., "A scanning tunneling microscope for surface science studies," *IBM J. Res. Dev.* **30**(4), 396–402 (1986).
3. G. N. Parsons et al., "History of atomic layer deposition and its relationship with the American Vacuum Society," *J. Vac. Sci. Technol. A* **31**(5), 050818 (2013).
4. J. I. Gittleman, B. Abeles, and S. Bozowski, "Superparamagnetism and relaxation effects in granular Ni-SiO_2 and Ni-Al_2O_3 films," *Phys. Rev. B* **9**(9), 3891–3897 (1974).
5. A. I. Ekimov, A. L. Efros, and A. A. Onushchenko, "Quantum size effect in semiconductor microcrystals," *Solid State Commun.* **56**(11), 921–924 (1985).
6. S. A. Maier, *Plasmonics: Fundamentals and Applications*, Springer, New York (2007).
7. M. L. Brongersma, J. W. Hartman, and H. H. Atwater, "Plasmonics: electromagnetic energy transfer and switching in nanoparticle chain-arrays below the diffraction limit," *MRS Online Proc. Libr.* **582**, 1–6 (1999).
8. H. A. Atwater, "The promise of plasmonics (cover story)," *Sci. Am.* **296**(4), 56–63 (2007).
9. M. L. Brongersma and V. M. Shalaev, "The case for plasmonics," *Science* **328**(5977), 440–441 (2010).
10. E. C. Le Ru and P. G. Etchegoin, "Introduction to plasmons and plasmonics," Chapter 3 in *Surface Enhanced Raman Spectroscopy and Related Plasmonics Effects*, E. C. Le Ru and P. G. Etchegoin, Eds., pp. 121–183, Elsevier, Amsterdam (2009).
11. C. L. Haynes and R. P. Van Duyne, "Nanosphere lithography: a versatile nanofabrication tool for studies of size-dependent nanoparticle optics," *J. Phys. Chem. B* **105**(24), 5599–5611 (2001).
12. C. J. Orendorff et al., "Aspect ratio dependence on surface enhanced Raman scattering using silver and gold nanorod substrates," *Phys. Chem. Chem. Phys.* **8**(1), 165–170 (2006).
13. G. H. Chan et al., "Localized surface plasmon resonance spectroscopy of triangular aluminum nanoparticles," *J. Phys. Chem. C* **112**(36), 13958–13963 (2008).
14. J. C. Fraire, L. A. Pérez, and E. A. Coronado, "Cluster size effects in the surface-enhanced Raman scattering response of Ag and Au nanoparticle aggregates: experimental and theoretical insight," *J. Phys. Chem. C* **117**(44), 23090–23107 (2013).
15. M. W. Knight et al., "Aluminum for plasmonics," *ACS Nano* **8**(1), 834–840 (2014).
16. J. M. McMahon, G. C. Schatz, and S. K. Gray, "Plasmonics in the ultraviolet with the poor metals Al, Ga, In, Sn, Tl, Pb, and Bi," *Phys. Chem. Chem. Phys.* **15**(15), 5415–5423 (2013).
17. S. Eustis and M. A. El-Sayed, "Determination of the aspect ratio statistical distribution of gold nanorods in solution from a theoretical fit of the observed inhomogeneously broadened longitudinal plasmon resonance absorption spectrum," *J. Appl. Phys.* **100**(4), 044324 (2006).
18. R. Boyack and E. C. Le Ru, "Investigation of particle shape and size effects in SERS using T-matrix calculations," *Phys. Chem. Chem. Phys.* **11**(34), 7398–7405 (2009).
19. "800 nm Resonant Gold Nanorods, Citrate-1 OD," http://50.87.149.212/_Specification%20Nanorods/800nm_Res_GNRs_Citrate_SDA0135_1OD_CoA-For%20Web%20Only.pdf?261%20502, (7 February 2015).
20. J. F. Wang et al., "Tunable surface-plasmon-resonance wavelength of silver island films," *Chin. Phys. B* **19**(11), 117310 (2010).
21. R. Gans, "Über die Form ultramikroskopischer Silberteilchen," *Ann. Phys.* **352**(10), 270–284 (1915).
22. M. Fleischmann, P. J. Hendra, and A. J. McQuillan, "Raman spectra of pyridine adsorbed at a silver electrode," *Chem. Phys. Lett.* **26**(2), 163–166 (1974).
23. D. L. Jeanmaire and R. P. Van Duyne, "Surface Raman spectroelectrochemistry: part I. Heterocyclic, aromatic, and aliphatic amines adsorbed on the anodized silver electrode," *J. Electroanal. Chem. Interfacial Electrochem.* **84**(1), 1–20 (1977).
24. M. G. Albrecht and J. A. Creighton, "Anomalously intense Raman spectra of pyridine at a silver electrode," *J. Am. Chem. Soc.* **99**(15), 5215–5217 (1977).
25. M. Moskovits, "Surface roughness and the enhanced intensity of Raman scattering by molecules adsorbed on metals," *J. Chem. Phys.* **69**(9), 4159–4161 (1978).
26. M. Moskovits, "How the localized surface plasmon became linked with surface-enhanced Raman spectroscopy," *Notes Rec. R. Soc.* **66**(2), 195–203 (2012).
27. J. Gersten and A. Nitzan, "Electromagnetic theory of enhanced Raman scattering by molecules adsorbed on rough surfaces," *J. Chem. Phys.* **73**(7), 3023–3037 (1980).
28. G. C. Schatz, "Theoretical studies of surface enhanced Raman scattering," *Acc. Chem. Res.* **17**(10), 370–376 (1984).
29. M. Moskovits, "Surface-enhanced spectroscopy," *Rev. Mod. Phys.* **57**(3), 783–826 (1985).
30. M. Moskovits, "Surface-enhanced Raman spectroscopy: a brief retrospective," *J. Raman Spectrosc.* **36**(6–7), 485–496 (2005).
31. K. Kneipp, M. Moskovits, and H. Kneipp, *Surface-Enhanced Raman Scattering: Physics and Applications*, Springer, Berlin, Heidelberg (2006).
32. E. C. Le Ru and P. G. Etchegoin, "SERS enhancement factors and related topics," Chapter 4 in *Surface Enhanced Raman Spectroscopy and Related Plasmonics Effects*, E. C. Le Ru and P. G. Etchegoin, Eds., pp. 185–264, Elsevier, Amsterdam (2009).
33. M. Moskovits, "Persistent misconceptions regarding SERS," *Phys. Chem. Chem. Phys.* **15**(15), 5301–5311 (2013).

34. H. Xu et al., "Electromagnetic contributions to single-molecule sensitivity in surface-enhanced Raman scattering," *Phys. Rev. E* **62**(3), 4318–4324 (2000).
35. W. E. Doering and S. Nie, "Single-molecule and single-nanoparticle SERS: examining the roles of surface active sites and chemical enhancement," *J. Phys. Chem. B* **106**(2), 311–317 (2002).
36. K. L. Kelly et al., "The optical properties of metal nanoparticles: the influence of size, shape, and dielectric environment," *J. Phys. Chem. B* **107**(3), 668–677 (2003).
37. S. Lal et al., "Profiling the near field of a plasmonic nanoparticle with Raman-based molecular rulers," *Nano Lett.* **6**(10), 2338–2343 (2006).
38. B. Sharma et al., "High-performance SERS substrates: advances and challenges," *MRS Bull.* **38**(8), 615–624 (2013).
39. K. Tanabe, "Field enhancement around metal nanoparticles and nanoshells: a systematic investigation," *J. Phys. Chem. C* **112**(40), 15721–15728 (2008).
40. S. K. Jha et al., "Deep-UV surface-enhanced resonance Raman scattering of adenine on aluminum nanoparticle arrays," *J. Am. Chem. Soc.* **134**(4), 1966–1969 (2012).
41. E. C. Le Ru et al., "Surface enhanced Raman scattering enhancement factors: a comprehensive study," *J. Phys. Chem. C* **111**(37), 13794–13803 (2007).
42. J. I. Gersten, "The effect of surface roughness on surface-enhanced Raman scattering," *J. Chem. Phys.* **72**(10), 5779–5780 (1980).
43. L. Ming et al., "Shape-dependent surface-enhanced Raman scattering in gold-Raman-probe-silica sandwiched nanoparticles for biocompatible applications," *Nanotechnology* **23**(11), 115501 (2012).
44. S. L. Smitha et al., "Gold nanorods with finely tunable longitudinal surface plasmon resonance as SERS substrates," *Nanotechnology* **22**(26), 265705 (2011).
45. S. Nie and S. R. Emory, "Probing single molecules and single nanoparticles by surface-enhanced Raman scattering," *Science* **275**(5303), 1102–1106 (1997).
46. K. Kneipp et al., "Single molecule detection using surface-enhanced Raman scattering (SERS)," *Phys. Rev. Lett.* **78**(9), 1667–1670 (1997).
47. K. Kneipp et al., "Extremely large enhancement factors in surface-enhanced Raman scattering for molecules on colloidal gold clusters," *Appl. Spectrosc.* **52**(12), 1493–1497 (1998).
48. E. Hao and G. C. Schatz, "Electromagnetic fields around silver nanoparticles and dimers," *J. Chem. Phys.* **120**(1), 357–366 (2004).
49. K. Kneipp et al., "Surface-enhanced Raman spectroscopy in single living cells using gold nanoparticles," *Appl. Spectrosc.* **56**(2), 150–154 (2002).
50. L. Gunnarsson et al., "Interparticle coupling effects in nanofabricated substrates for surface-enhanced Raman scattering," *Appl. Phys. Lett.* **78**(6), 802–804 (2001).
51. R. P. Van Duyne, J. C. Hulteen, and D. A. Treichel, "Atomic force microscopy and surface-enhanced Raman spectroscopy. I. Ag island films and Ag film over polymer nanosphere surfaces supported on glass," *J. Chem. Phys.* **99**(3), 2101–2115 (1993).
52. A. Ibrahim et al., "Determination of enhancement factors for surface-enhanced FT-Raman spectroscopy on gold and silver surfaces," *J. Raman Spectrosc.* **27**(12), 887–891 (1996).
53. L. Bao, S. M. Mahurin, and S. Dai, "Controlled layer-by-layer formation of ultrathin TiO_2 on silver island films via a surface sol–gel method for surface-enhanced Raman scattering measurement," *Anal. Chem.* **76**(15), 4531–4536 (2004).
54. T. Vo-Dinh et al., "Surface-enhanced Raman spectrometry for trace organic analysis," *Anal. Chem.* **56**(9), 1667–1670 (1984).
55. J. C. Hulteen et al., "Nanosphere lithography: size-tunable silver nanoparticle and surface cluster arrays," *J. Phys. Chem. B* **103**(19), 3854–3863 (1999).
56. A. D. McFarland et al., "Wavelength-scanned surface-enhanced Raman excitation spectroscopy," *J. Phys. Chem. B* **109**(22), 11279–11285 (2005).
57. H. Li and B. M. Cullum, "Dual layer and multilayer enhancements from silver film over nanostructured surface-enhanced Raman substrates," *Appl. Spectrosc.* **59**(4), 410–417 (2005).
58. "Klarite™—substrates for surface enhanced Raman scattering" (2010), http://resources.renishaw.com/en/details/klarite-datasheet-26857 (7 February 2015).
59. K. Kneipp et al., "Detection and identification of a single DNA base molecule using surface-enhanced Raman scattering (SERS)," *Phys. Rev. E* **57**(6), R6281–R6284 (1998).
60. H. Yuan et al., "Spectral characterization and intracellular detection of surface-enhanced Raman scattering (SERS)-encoded plasmonic gold nanostars," *J. Raman Spectrosc.* **44**(2), 234–239 (2013).
61. C. McLaughlin, D. Graham, and W. E. Smith, "Comparison of resonant and non resonant conditions on the concentration dependence of surface enhanced Raman scattering from a dye adsorbed on silver colloid," *J. Phys. Chem. B* **106**(21), 5408–5412 (2002).
62. J. B. Jackson and N. J. Halas, "Surface-enhanced Raman scattering on tunable plasmonic nanoparticle substrates," *Proc. Natl. Acad. Sci. U. S. A.* **101**(52), 17930–17935 (2004).
63. J. B. Jackson and N. J. Halas, "Silver nanoshells: variations in morphologies and optical properties," *J. Phys. Chem. B* **105**(14), 2743–2746 (2001).
64. C. E. Talley et al., "Surface-enhanced Raman scattering from individual Au nanoparticles and nanoparticle dimer substrates," *Nano Lett.* **5**(8), 1569–1574 (2005).
65. S. J. Oldenburg et al., "Nanoengineering of optical resonances," *Chem. Phys. Lett.* **288**(2–4), 243–247 (1998).
66. J. D. Driskell et al., "The use of aligned silver nanorod arrays prepared by oblique angle deposition as surface enhanced Raman scattering substrates," *J. Phys. Chem. C* **112**(4), 895–901 (2008).
67. N. G. Greeneltch et al., "Plasmon-sampled surface-enhanced Raman excitation spectroscopy on silver immobilized nanorod assemblies and optimization for near infrared (λ_{ex} = 1064 nm) studies," *J. Phys. Chem. C* **117**(6), 2554–2558 (2013).
68. K. D. Osberg et al., "Dispersible gold nanorod dimers with sub-5 nm gaps as local amplifiers for surface-enhanced Raman scattering," *Nano Lett.* **12**(7), 3828–3832 (2012).
69. M. Hu et al., "Gold nanofingers for molecule trapping and detection," *J. Am. Chem. Soc.* **132**(37), 12820–12822 (2010).
70. S. J. Oldenburg et al., "Surface enhanced Raman scattering in the near infrared using metal nanoshell substrates," *J. Chem. Phys.* **111**(10), 4729–4735 (1999).
71. X. Zhang et al., "Ultrastable substrates for surface-enhanced Raman spectroscopy: Al_2O_3 overlayers fabricated by atomic layer deposition yield improved anthrax biomarker detection," *J. Am. Chem. Soc.* **128**(31), 10304–10309 (2006).
72. M. Roca and A. J. Haes, "Silica-void-gold nanoparticles: temporally stable surface-enhanced Raman scattering substrates," *J. Am. Chem. Soc.* **130**(43), 14273–14279 (2008).
73. J. F. Li et al., "Shell-isolated nanoparticle-enhanced Raman spectroscopy," *Nature* **464**(7287), 392–395 (2010).
74. X.-D. Lin et al., "Shell-isolated nanoparticle-enhanced Raman spectroscopy: nanoparticle synthesis, characterization and applications in electrochemistry," *J. Electroanal. Chem.* **688**, 5–11 (2013).
75. X. Li et al., "Ordered array of gold semishells on TiO_2 spheres: an ultrasensitive and recyclable SERS substrate," *ACS Appl. Mater. Interfaces* **4**(4), 2180–2185 (2012).
76. Y. Zhao et al., "Electrospun TiO_2 nanofelt surface-decorated with Ag nanoparticles as sensitive and UV-cleanable substrate for surface enhanced Raman scattering," *ACS Appl. Mater. Interfaces* **6**(8), 5759–5767 (2014).
77. C. L. Leverette et al., "Development of a novel dual-layer thick Ag substrate for surface-enhanced Raman scattering (SERS) of self-assembled monolayers," *J. Phys. Chem. B* **106**(34), 8747–8755 (2002).
78. H. Li et al., "Multilayer enhanced gold film over nanostructure surface-enhanced Raman substrates," *Appl. Spectrosc.* **60**(12), 1377–1385 (2006).
79. B. M. Cullum et al., "Characterization of multilayer-enhanced surface-enhanced Raman scattering (SERS) substrates and their potential for SERS nanoimaging," *NanoBiotechnology* **3**(1), 1–11 (2007).
80. H. Im et al., "Self-assembled plasmonic nanoring cavity arrays for SERS and LSPR biosensing," *Adv. Mater.* **25**(19), 2678–2685 (2013).
81. T. Pham et al., "Preparation and characterization of gold nanoshells coated with self-assembled monolayers," *Langmuir* **18**(12), 4915–4920 (2002).
82. E. Prodan et al., "A hybridization model for the plasmon response of complex nanostructures," *Science* **302**(5644), 419–422 (2003).
83. M. Culha et al., "Surface-enhanced Raman scattering as an emerging characterization and detection technique," *J. Nanotechnol.* **2012**, 15 (2012).
84. P. Strobbia et al., "Characterization of the role of oxide spacers in multilayer-enhanced SERS probes," *Proc. SPIE* **9487**, 94870P (2015).
85. S. B. Chaney et al., "Aligned silver nanorod arrays produce high sensitivity surface-enhanced Raman spectroscopy substrates," *Appl. Phys. Lett.* **87**(3), 031908 (2005).
86. M. E. Hankus et al., "Surface-enhanced Raman scattering-based nanoprobe for high-resolution, non-scanning chemical imaging," *Anal. Chem.* **78**(21), 7535–7546 (2006).
87. C. G. Khoury and T. Vo-Dinh, "Gold nanostars for surface-enhanced Raman scattering: synthesis, characterization and optimization," *J. Phys. Chem. C* **112**(48), 18849–18859 (2008).
88. R. Sardar and J. S. Shumaker-Parry, "Asymmetrically functionalized gold nanoparticles organized in one-dimensional chains," *Nano Lett.* **8**(2), 731–736 (2008).
89. R. Sardar, T. B. Heap, and J. S. Shumaker-Parry, "Versatile solid phase synthesis of gold nanoparticle dimers using an asymmetric functionalization approach," *J. Am. Chem. Soc.* **129**(17), 5356–5357 (2007).
90. L. Qin et al., "Designing, fabricating, and imaging Raman hot spots," *Proc. Natl. Acad. Sci. U. S. A.* **103**(36), 13300–13303 (2006).
91. M. Pilo-Pais et al., "Surface-enhanced Raman scattering plasmonic enhancement using DNA origami-based complex metallic nanostructures," *Nano Lett.* **14**(4), 2099–2104 (2014).
92. D. Graham et al., "Control of enhanced Raman scattering using a DNA-based assembly process of dye-coded nanoparticles," *Nat. Nano* **3**(9), 548–551 (2008).

93. M. A. Penn, D. M. Drake, and J. D. Driskell, "Accelerated surface-enhanced Raman spectroscopy (SERS)-based immunoassay on a gold-plated membrane," *Anal. Chem.* **85**(18), 8609–8617 (2013).
94. N. H. Kim, S. J. Lee, and M. Moskovits, "Aptamer-mediated surface-enhanced Raman spectroscopy intensity amplification," *Nano Lett.* **10**(10), 4181–4185 (2010).
95. H. T. Ngo et al., "Label-free DNA biosensor based on SERS molecular sentinel on nanowave chip," *Anal. Chem.* **85**(13), 6378–6383 (2013).
96. R. Elghanian et al., "Selective colorimetric detection of polynucleotides based on the distance-dependent optical properties of gold nanoparticles," *Science* **277**(5329), 1078–1081 (1997).
97. Y. Kim, R. C. Johnson, and J. T. Hupp, "Gold nanoparticle-based sensing of 'spectroscopically silent' heavy metal ions," *Nano Lett.* **1**(4), 165–167 (2001).
98. A. Otto, "Excitation of nonradiative surface plasma waves in silver by the method of frustrated total reflection," *Z. Phys.* **216**(4), 398–410 (1968).
99. E. Kretschmann and H. Raether, "Notizen: radiative decay of non radiative surface plasmons excited by light," *Z. Nat. A* **23**, 2135 (1968).
100. H. N. Daghestani and B. W. Day, "Theory and applications of surface plasmon resonance, resonant mirror, resonant waveguide grating, and dual polarization interferometry biosensors," *Sensors* **10**(11), 9630 (2010).
101. Y. Chen and H. Ming, "Review of surface plasmon resonance and localized surface plasmon resonance sensor," *Photonic Sens.* **2**(1), 37–49 (2012).
102. J. Homola, S. S. Yee, and G. Gauglitz, "Surface plasmon resonance sensors: review," *Sens. Actuators B* **54**(1–2), 3–15 (1999).
103. B. D. Gupta and R. K. Verma, "Surface plasmon resonance-based fiber optic sensors: principle, probe designs, and some applications," *J. Sens.* **2009**, 12 (2009).
104. C. Wong and M. Olivo, "Surface plasmon resonance imaging sensors: a review," *Plasmonics* **9**(4), 809–824 (2014).
105. R. C. Jorgenson and S. S. Yee, "A fiber-optic chemical sensor based on surface plasmon resonance," *Sens. Actuators B* **12**(3), 213–220 (1993).
106. L. A. Obando and K. S. Booksh, "Tuning dynamic range and sensitivity of white-light, multimode, fiber-optic surface plasmon resonance sensors," *Anal. Chem.* **71**(22), 5116–5122 (1999).
107. L. S. Live, O. R. Bolduc, and J.-F. Masson, "Propagating surface plasmon resonance on microhole arrays," *Anal. Chem.* **82**(9), 3780–3787 (2010).
108. M. Couture et al., "Tuning the 3D plasmon field of nanohole arrays," *Nanoscale* **5**(24), 12399–12408 (2013).
109. Y. Lin et al., "E-beam patterned gold nanodot arrays on optical fiber tips for localized surface plasmon resonance biochemical sensing," *Sensors* **10**(10), 9397–9406 (2010).
110. J. Parsons et al., "Localized surface-plasmon resonances in periodic nondiffracting metallic nanoparticle and nanohole arrays," *Phys. Rev. B* **79**(7), 073412 (2009).
111. A. Karabchevsky, M. Auslender, and I. Abdulhalim, "Dual-surface plasmon excitation with thin metallic nanoslits," *J. Nanophotonics* **5**(1), 051821 (2011).
112. J. Fischer et al., "Plasmon hybridization and strong near-field enhancements in opposing nanocrescent dimers with tunable resonances," *Nanoscale* **3**(11), 4788–4797 (2011).
113. N. Vogel et al., "Plasmon hybridization in stacked double crescents arrays fabricated by colloidal lithography," *Nano Lett.* **11**(2), 446–454 (2011).
114. J. Zeng et al., "Morphological control and plasmonic tuning of nanoporous gold disks by surface modifications," *J. Mater. Chem. C* **3**(2), 247–252 (2015).
115. F. Zhao et al., "Monolithic NPG nanoparticles with large surface area, tunable plasmonics, and high-density internal hot-spots," *Nanoscale* **6**(14), 8199–8207 (2014).
116. M. D. Baiad and R. Kashyap, "Concatenation of surface plasmon resonance sensors in a single optical fiber using tilted fiber Bragg gratings," *Opt. Lett.* **40**(1), 115–118 (2015).
117. I. Abdulhalim, M. Auslender, and S. Hava, "Resonant and scatterometric grating-based nanophotonic structures for biosensing," *J. Nanophotonics* **1**(1), 011680 (2007).
118. M. Couture et al., "EOT or Kretschmann configuration? Comparative study of the plasmonic modes in gold nanohole arrays," *Analyst* **137**(18), 4162–4170 (2012).
119. L. Live et al., "Angle-dependent resonance of localized and propagating surface plasmons in microhole arrays for enhanced biosensing," *Anal. Bioanal.Chem.* **404**(10), 2859–2868 (2012).
120. L. L. Kegel, D. Boyne, and K. S. Booksh, "Sensing with prism-based near-infrared surface plasmon resonance spectroscopy on nanohole array platforms," *Anal. Chem.* **86**(7), 3355–3364 (2014).
121. F. Zhao et al., "In situ patterning of hierarchical nanoporous gold structures by in-plane dealloying," *Mater. Sci. Eng. B* **194**, 34–40 (2015).
122. W. Peng et al., "Metallic nanowire array-polymer hybrid film for surface plasmon resonance sensitivity enhancement and spectral range enlargement," *Plasmonics* **9**(2), 319–326 (2014).
123. K. H. Drexhage, "Chapter IV Interaction of light with monomolecular dye layers," in *Progress in Optics*, K. H. Drexhage, Eds., pp. 163–232, Elsevier, Amsterdam, Netherlands (1974).
124. M. R. Philpott, "Effect of surface plasmons on transitions in molecules," *J. Chem. Phys.* **62**(5), 1812–1817 (1975).
125. H. Kuhn, "Classical aspects of energy transfer in molecular systems," *J. Chem. Phys.* **53**(1), 101–108 (1970).
126. C. Geddes and J. Lakowicz, "Editorial: metal-enhanced fluorescence," *J. Fluorescence* **12**(2), 121–129 (2002).
127. J. R. Lakowicz, "Radiative decay engineering: biophysical and biomedical applications," *Anal. Biochem.* **298**(1), 1–24 (2001).
128. J. R. Lakowicz et al., "Intrinsic fluorescence from DNA can be enhanced by metallic particles," *Biochem. Biophys. Res. Commun.* **286**(5), 875–879 (2001).
129. K. Aslan and C. D. Geddes, "Metal-enhanced fluorescence: progress towards a unified plasmon-fluorophore description," Chapter 1 in *Metal-Enhanced Fluorescence: Progress Towards a Unified Plasmon-Fluorophore Description*, K. Aslan and C. D. Geddes, Eds., pp. 1–23, John Wiley & Sons, Inc., Hoboken, New Jersey (2010).
130. C. D. Geddes, *Metal-Enhanced Fluorescence*, John Wiley & Sons, Hoboken, New Jersey (2010).
131. E. C. L. Ru et al., "Spectral profile modifications in metal-enhanced fluorescence," Chapter 2 in *Spectral Profile Modifications in Metal-Enhanced Fluorescence*, E. C. L. Ru et al., Eds., pp. 25–65, John Wiley & Sons, Inc., Hoboken, New Jersey (2010).
132. R. Carminati et al., "Radiative and non-radiative decay of a single molecule close to a metallic nanoparticle," *Opt. Commun.* **261**(2), 368–375 (2006).
133. J. Kümmerlen et al., "Enhanced dye fluorescence over silver island films: analysis of the distance dependence," *Mol. Phys.* **80**(5), 1031–1046 (1993).
134. K. Munechika et al., "Importance of spectral overlap: fluorescence enhancement by single metal nanoparticles," Chapter4 in *Importance of Spectral Overlap: Fluorescence Enhancement by Single Metal Nanoparticles*, K. Munechika et al., Eds., pp. 91–118, John Wiley & Sons, Inc., Hoboken, New Jersey (2010).
135. Y. Chen, K. Munechika, and D. S. Ginger, "Dependence of fluorescence intensity on the spectral overlap between fluorophores and plasmon resonant single silver nanoparticles," *Nano Lett.* **7**(3), 690–696 (2007).
136. Á. Sánchez-González, S. Corni, and B. Mennucci, "Surface-enhanced fluorescence within a metal nanoparticle array: the role of solvent and plasmon couplings," *J. Phys. Chem. C* **115**(13), 5450–5460 (2011).
137. A. I. Dragan and C. D. Geddes, "Metal-enhanced fluorescence: the role of quantum yield, Q0, in enhanced fluorescence," *Appl. Phys. Lett.* **100**(9), 093115 (2012).
138. J. Karolin and C. Geddes, "Reduced lifetimes are directly correlated with excitation irradiance in metal-enhanced fluorescence (MEF)," *J. Fluoresc.* **22**(6), 1659–1662 (2012).
139. G. Ritchie and E. Burstein, "Luminescence of dye molecules adsorbed at a Ag surface," *Phys. Rev. B* **24**(8), 4843–4846 (1981).
140. A. M. Glass et al., "Interaction of metal particles with adsorbed dye molecules: absorption and luminescence," *Opt. Lett.* **5**(9), 368–370 (1980).
141. B.-Y. Hsieh et al., "Localized surface plasmon coupled fluorescence fiber-optic biosensor with gold nanoparticles," *Anal. Chem.* **79**(9), 3487–3493 (2007).
142. D. Darvill, A. Centeno, and F. Xie, "Plasmonic fluorescence enhancement by metal nanostructures: shaping the future of bionanotechnology," *Phys. Chem. Chem. Phys.* **15**(38), 15709–15726 (2013).
143. W. Deng et al., "Metal-enhanced fluorescence in the life sciences: here, now and beyond," *Phys. Chem. Chem. Phys.* **15**(38), 15695–15708 (2013).
144. A. I. Dragan et al., "Metal-enhanced PicoGreen® fluorescence: application to fast and ultra-sensitive pg/ml DNA quantitation," *J. Immunol. Methods* **362**(1–2), 95–100 (2010).
145. S. M. Tennant et al., "Ultra-fast and sensitive detection of non-typhoidal salmonella using microwave-accelerated metal-enhanced fluorescence ("MAMEF")," *PLoS One* **6**(4), e18700 (2011).
146. K. Aslan et al., "Metal-enhanced fluorescence: an emerging tool in biotechnology," *Curr. Opin. Biotechnol.* **16**(1), 55–62 (2005).
147. H. Szmacinski et al., "Imaging of protein secretion from a single cell using plasmonic substrates," *Bionanoscience* **3**(1), 30–36 (2013).
148. K. Aslan et al., "Metal-enhanced fluorescence solution-based sensing platform," *J. Fluoresc.* **14**(6), 677–679 (2004).
149. Q. Cui et al., "Controllable metal-enhanced fluorescence in organized films and colloidal system," *Adv. Colloid Interface Sci.* **207**, 164–177 (2014).
150. C. D. Geddes et al., "Metal-enhanced fluorescence (MEF) due to silver colloids on a planar surface: potential applications of indocyanine green to in vivo imaging†," *J. Phys. Chem. A* **107**(18), 3443–3449 (2003).
151. P. P. Pompa et al., "Metal-enhanced fluorescence of colloidal nanocrystals with nanoscale control," *Nat. Nano* **1**(2), 126–130 (2006).
152. Y. Zhang et al., "Metal-enhanced fluorescence from paper substrates: modified spectral properties of dyes for potential high-throughput surface analysis and assays and as an anti-counterfeiting technology," *Dyes Pigm.* **77**(3), 545–549 (2008).
153. K. Aslan, J. R. Lakowicz, and C. D. Geddes, "Rapid deposition of triangular silver nanoplates on planar surfaces: application to metal-enhanced fluorescence," *J. Phys. Chem. B* **109**(13), 6247–6251 (2005).

154. K. Aslan et al., "Extraction and detection of DNA from Bacillus anthracis spores and the vegetative cells within 1 min," *Anal. Chem.* **80**(11), 4125–4132 (2008).
155. T. Shtoyko et al., "Enhanced fluorescent immunoassays on silver fractal-like structures," *Anal. Chem.* **80**(6), 1962–1966 (2008).
156. L. Zhang et al., "Large enhancement of quantum dot fluorescence by highly scalable nanoporous gold," *Adv. Mater.* **26**(8), 1289–1294 (2014).
157. E. Hwang, I. I. Smolyaninov, and C. C. Davis, "Surface plasmon polariton enhanced fluorescence from quantum dots on nanostructured metal surfaces," *Nano Lett.* **10**(3), 813–820 (2010).
158. L. Langguth et al., "Plasmonic band structure controls single-molecule fluorescence," *ACS Nano* **7**(10), 8840–8848 (2013).
159. H. Aouani et al., "Bright unidirectional fluorescence emission of molecules in a nanoaperture with plasmonic corrugations," *Nano Lett.* **11**(2), 637–644 (2011).
160. D. Punj et al., "A plasmonic 'antenna-in-box' platform for enhanced single-molecule analysis at micromolar concentrations," *Nat. Nanotechnol.* **8**(7), 512–516 (2013).
161. F. Xie et al., "Nanoscale control of Ag nanostructures for plasmonic fluorescence enhancement of near-infrared dyes," *Nano Res.* **6**(7), 496–510 (2013).
162. Z. Xu et al., "Surface plasmon enhanced broadband spectrophotometry on black silver substrates," *Appl. Phys. Lett.* **98**(24), 241904 (2011).
163. S. Dutta Choudhury et al., "Silver-gold nanocomposite substrates for metal-enhanced fluorescence: ensemble and single-molecule spectroscopic studies," *J. Phys. Chem. C* **116**(8), 5042–5048 (2012).
164. X. Li et al., "Aluminum oxide nanostructure-based substrates for fluorescence enhancement," *Opt. Express* **20**(19), 21272–21277 (2012).
165. H. Jun-wei et al., "Synthesis of silver particles decorated anodic aluminium oxide substrates for metal-enhanced fluorescencer," *Micro Nano Lett.* **7**(8), 842–845 (2012).
166. K. Sugawa et al., "Metal-enhanced fluorescence platforms based on plasmonic ordered copper arrays: wavelength dependence of quenching and enhancement effects," *ACS Nano* **7**(11), 9997–10010 (2013).
167. X. Tian et al., "Modulated fluorescence properties in fluorophore-containing gold nanorods@mSiO_2," *RSC Adv.* **4**(18), 9343–9348 (2014).
168. A. M. Gabudean, D. Biro, and S. Astilean, "Hybrid plasmonic platforms based on silica-encapsulated gold nanorods as effective spectroscopic enhancers for Raman and fluorescence spectroscopy," *Nanotechnology* **23**(48), 485706 (2012).
169. A. M. Gabudean, M. Focsan, and S. Astilean, "Gold nanorods performing as dual-modal nanoprobes via metal-enhanced fluorescence (MEF) and surface-enhanced Raman scattering (SERS)," *J. Phys. Chem. C* **116**(22), 12240–12249 (2012).
170. C. Xiao et al., "Microfluidic-based metal enhanced fluorescence for capillary electrophoresis by Ag nanorod arrays," *Nanotechnology* **25**(22), 225502 (2014).
171. D. Yin et al., "Preparation of a novel core-shell Ag-graphene@SiO_2 nanocomposite for fluorescence enhancement," *J. Biomed. Nanotechnol.* **8**(3), 458–464 (2012).
172. E. Jang, K. Son, and W. G. Koh, "Metal-enhanced fluorescence using silver nanoparticles-embedded polyelectrolyte multilayer films for microarray-based immunoassays," *Colloids Polym. Sci.* **292**(6), 1355–1364 (2014).
173. H. Cheng et al., "Gold nanoparticle-enhanced near infrared fluorescent nanocomposites for targeted bio-imaging," *RSC Adv.* **5**(1), 20–26 (2015).
174. Y. K. Xu et al., "Two orders of magnitude fluorescence enhancement of aluminum phthalocyanines by gold nanocubes: a remarkable improvement for cancer cell imaging and detection," *ACS Appl. Mater. Interfaces* **6**(8), 5619–5628 (2014).
175. Y. Jiang et al., "Surface plasmon enhanced fluorescence of dye molecules on metal grating films," *J. Phys. Chem. C* **115**(25), 12636–12642 (2011).
176. X. Li, Y. He, and L. Que, "Fluorescence detection and imaging of biomolecules using the micropatterned nanostructured aluminum oxide," *Langmuir* **29**(7), 2439–2445 (2013).
177. N. Akbay et al., "Metal-enhanced intrinsic fluorescence of nucleic acids using platinum nanostructured substrates," *Chem. Phys. Lett.* **548**, 45–50 (2012).
178. A. Kinkhabwala et al., "Large single-molecule fluorescence enhancements produced by a bowtie nanoantenna," *Nat. Photonics* **3**(11), 654–657 (2009).
179. X. Yang et al., "Nanopillar array on a fiber facet for highly sensitive surface-enhanced Raman scattering," *Opt. Express* **20**(22), 24819–24826 (2012).
180. S. Chaudhary et al., "Controlled short-linkage assembly of functional nano-objects," *Appl. Surf. Sci.* **300**, 22–28 (2014).
181. H. Sharma et al., "Shrink-induced silica multiscale structures for enhanced fluorescence from DNA microarrays," *Langmuir* **30**(37), 10979–10983 (2014).
182. H. Sharma et al., "Enhanced emission of fluorophores on shrink-induced wrinkled composite structures," *Opt. Mater. Express* **4**(4), 753–763 (2014).
183. A. Li et al., "Design and synthesis of fluorescent core–shell nanoparticles with tunable lower critical solution temperature behavior and metal-enhanced fluorescence," *J. Polym. Sci. Part A* **52**(1), 87–95 (2014).
184. F. Tang et al., "Control of metal-enhanced fluorescence with pH- and thermoresponsive hybrid microgels," *Langmuir* **28**(1), 883–888 (2012).
185. R. Contreras-Caceres et al., "Temperature controlled fluorescence on Au@Ag@PNIPAM-PTEBS microgels: effect of the metal core size on the MEF extension," *Langmuir* **30**(51), 15560–15567 (2014).

Biographies for the authors are not available.